Small-Molecule Screen Identifies Reactive Oxygen Species as Key Regulators of Neutrophil Chemotaxis

Small-molecule screen identifies reactive oxygen species as key regulators of neutrophil chemotaxis

Hidenori Hattori[a,1], Kulandayan K. Subramanian[a,1], Jiro Sakai[a,1], Yonghui Jia[a], Yitang Li[a], Timothy F. Porter[b], Fabien Loison[a], Bara Sarraj[a], Anongnard Kasorn[a], Hakryul Jo[a], Catlyn Blanchard[a], Dorothy Zirkle[a], Douglas McDonald[c], Sung-Yun Pai[d], Charles N. Serhan[b], and Hongbo R. Luo[a,2]

[a]Department of Pathology, Harvard Medical School Dana–Farber/Harvard Cancer Center and Department of Laboratory Medicine, Children's Hospital Boston, Boston, MA 02115; [b]Center for Experimental Therapeutics and Reperfusion Injury, Department of Anesthesiology, Perioperative and Pain Medicine, Brigham and Women's Hospital and Harvard Medical School, Boston, MA 02115; [c]Division of Immunology, Children's Hospital Boston, and Department of Pediatrics, Harvard Medical School, Boston, MA 02115; and [d]Combined Department of Pediatric Hematology–Oncology, Children's Hospital Boston and Dana-Farber Cancer Institute, Harvard Medical School, Boston, MA 02115

Edited* by Solomon Snyder, Johns Hopkins University School of Medicine, Baltimore, MD, and approved January 15, 2010 (received for review December 11, 2009)

Neutrophil chemotaxis plays an essential role in innate immunity, but the underlying cellular mechanism is still not fully characterized. Here, using a small-molecule functional screening, we identified NADPH oxidase–dependent reactive oxygen species as key regulators of neutrophil chemotactic migration. Neutrophils with pharmacologically inhibited oxidase, or isolated from chronic granulomatous disease (CGD) patients and mice, formed more frequent multiple pseudopodia and lost their directionality as they migrated up a chemoattractant concentration gradient. Knocking down NADPH oxidase in differentiated neutrophil-like HL60 cells also led to defective chemotaxis. Consistent with the in vitro results, adoptively transferred CGD murine neutrophils showed impaired in vivo recruitment to sites of inflammation. Together, these results present a physiological role for reactive oxygen species in regulating neutrophil functions and shed light on the pathogenesis of CGD.

chronic granulomatous disease | innate immunity | NADPH oxidase

Neutrophils are major players in innate immunity and constitute the first line of host defense against invading bacteria and other pathogens. In response to inflammatory stimuli, neutrophils migrate from the blood to infected tissues, where they protect their host by engulfing, killing, and digesting invading bacterial and fungal pathogens. Conversely, excessive neutrophil accumulation can be detrimental to the system. Hence, neutrophil recruitment in response to inflammatory stimuli needs to be well controlled.

Neutrophils are recruited to the site of infection by responding to a variety of chemokines, leukotrienes, complement peptides, and some chemicals released by bacteria directly, such as peptides bearing the N-formyl group (i.e., formyl-peptides). Neutrophil chemotaxis is mediated by heterotrimeric guanine nucleotide-binding regulatory proteins (G protein)–coupled receptors (GPCRs). One essential downstream target of GPCR is PtdIns (3,4,5)P3. Chemoattractants bind receptors on cell membrane and induce the dissociation of a specific G protein into α- and βγ-subunits. Released βγ-subunits initiate accumulation of PtdIns (3,4,5)P3 and subsequent actin polymerization at the leading edge of chemotaxing cells. Earlier studies have suggested that PtdIns (3,4,5)P3 plays the essential role of a cellular compass, localizing to the leading edge of pseudopodia, mediating direction sensing during chemotactic migration and cell polarity (1–4). However, several recent studies have shown that loss of PI3K and reduced PtdIns(3,4,5)P3 level lead to decreased polarity, but does not affect the ability of the cell to sense chemoattractant gradients. In both human neutrophils (5, 6) and *Dictyostelium* (7–9), chemotaxis could occur independently of the PI3K-dependent actin polymerization, although it was somewhat delayed, suggesting extra pathways are required for neutrophil chemotaxis.

To identify these putative signal-induced chemotactic pathways, we conducted a functional screening for chemical compounds that disrupt neutrophil directionality. We have identified NADPH oxidase dependent reactive oxygen species (ROS) as key regulators of neutrophil chemotaxis. Neutrophils with pharmacologically inhibited NADPH oxidase, or isolated from chronic granulomatous disease (CGD) patients and mice, displayed more frequent multiple pseudopodia formation and impaired directionality during chemotaxis. This finding provides a cellular mechanism for CGD pathogenesis and might lead to development of new therapeutic strategies for this disease.

Results

Screening for Inhibitors of Neutrophil Chemotaxis. The screening was performed using an EZ-TAXIScan chemotaxis device in which a stable chemoattractant gradient was formed in a 260-μm–wide channel (Fig. S1*A*). Freshly purified human primary neutrophils migrated robustly up the gradient and most cells crossed the channel in 20 min (Fig. S1*B*). A Tocris screening library containing 386 biologically active compounds was used for screening (Table S1). To achieve the maximal inhibition of each targeted pathway in the primary screening, we treated neutrophils with each drug at a concentration equivalent to 10 times the IC_{50} of the drug. Although most compounds did not affect neutrophil chemotaxis (Dataset S1), 83 compounds displayed inhibitory effects. (The video files for each compound will be released to a public database after the publication of this article.) The inhibitory effects were elicited via a variety of mechanisms (Table S1), such as induction of cell death (Dataset S2), complete inhibition of polarization and migration, slow migration, and impairment of directionality. Selected compounds from the primary screen were then used at 0.2 to 10 times the IC_{50} in a secondary screening (Dataset S3). Most positive compounds identified from the primary screening showed the same inhibitory effect at lower concentrations, suggesting that the drug-induced phenotype changes were most likely caused by specific inhibition of each targeted pathway.

Author contributions: H.H., K.K.S., J.S., C.N.S., and H.R.L. designed research; H.H., K.K.S., J.S., Y.J., Y.L., T.F.P., F.L., B.S., A.K., H.J., C.B., and D.Z. performed research; D.M. and S.-Y.P. contributed new reagents/analytic tools; H.H., K.K.S., J.S., Y.J., Y.L., T.F.P., F.L., B.S., A.K., H.J., C.N.S., and H.R.L. analyzed data; and H.R.L. wrote the paper.

The authors declare no conflict of interest.

*This Direct Submission article had a prearranged editor.

Freely available online through the PNAS open access option.

[1]H.H., K.K.S., and J.S. contributed equally to this work.

[2]To whom correspondence should be addressed. E-mail: hongbo.luo@childrens.harvard.edu.

This article contains supporting information online at www.pnas.org/cgi/content/full/0914351107/DCSupplemental.

www.pnas.org/cgi/doi/10.1073/pnas.0914351107

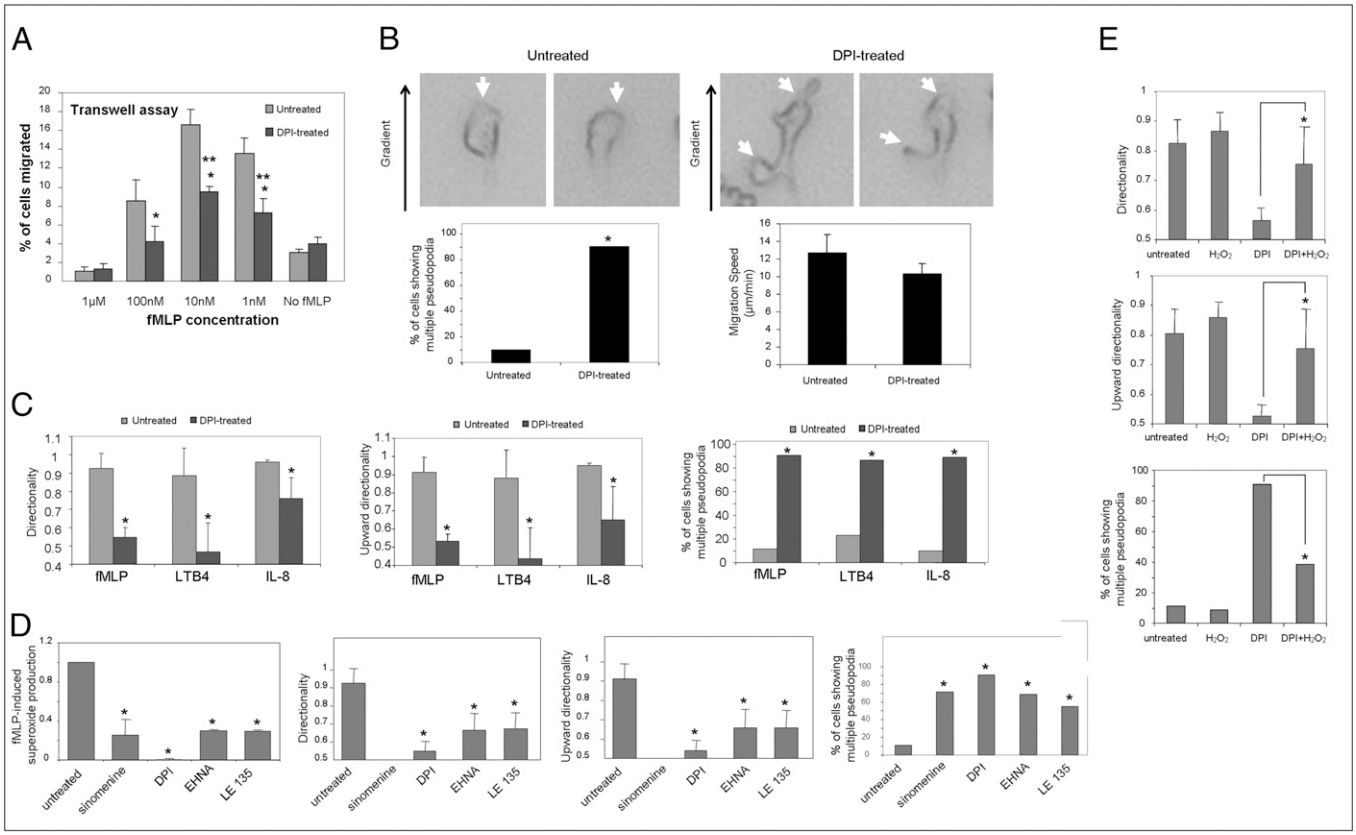

Fig. 1. Pharmacological inhibition of NADPH oxidase–mediated ROS production in human neutrophils leads to more frequent formation of multiple pseudopodia and reduced chemotaxis efficiency. (*A*) Inhibition of NADPH oxidase decreases transwell migration of human neutrophils. Human neutrophils were left untreated or pretreated with 50 μM DPI for 30 min at 37 °C, and then allowed to migrate in response to the indicated concentration of fMLP. Percentage of cells that migrated into the bottom well was recorded. Data shown are means ± SD from $n = 3$ wells, from one experiment representative of three. (*$P < 0.05$ vs. untreated neutrophils.) (*B*) Chemotaxing NADPH oxidase–inhibited human neutrophils display multiple pseudopodia more frequently, but do not show difference in cell speed. Representative images of human neutrophils treated (*Right*) or not treated (*Left*) with 50 μM DPI and allowed to chemotax in response to a chemoattractant gradient generated by addition of 1 μL of 100 nM fMLP in the EZ-TAXIScan device. White arrowheads specify pseudopodia in the cells. Percentage of cells that display multiple pseudopodia (bottom left, $n = 20$ cells; Fisher 2×2 test, *$P < 0.05$ vs. untreated) and migration speed (bottom right, mean ± SD from $n = 20$ cells; Student t test, *$P > 0.05$ vs. untreated) during the course of the EZ-TAXIScan chemotaxis assay in the DPI-treated or untreated case were quantified as described in *Experimental Procedures*. (*C*) Inhibition of NADPH oxidase leads to multiple pseudopod formation and defective directionality in fMLP-, LTB4-, and IL-8–mediated chemotaxis. Neutrophil chemotaxis in response to addition of 100 nM fMLP, 100 nM LTB4, or 10 nM IL-8 (1 μL each), with 50 μM DPI treatment (or without treatment), was analyzed ($n = 20$ cells) for directionality, upward directionality, and percentage of neutrophils displaying multiple pseudopodia as described earlier ($n = 20$ cells, *$P < 0.05$). (*D*) Pharmacological agents that inhibit ROS production cause chemotaxis defect in human neutrophils. fMLP-induced ROS production (Fig. S5 *Top*) in human neutrophils (5×10^5) pretreated with sinomenine (10 μM), DPI (50 μM), EHNA hydrochloride (40 μM), or LE135 (14 μM), or without pretreatment, was evaluated by stimulating neutrophils with 100 nM fMLP and monitoring chemiluminescence (for 1 s) every 7 s for 280 s, in the presence of 50 μM luminol and 0.8 U HRP in a luminometer at 37 °C. Data represent maximal chemiluminescence in drug-treated neutrophils normalized to maximal chemiluminescence in untreated neutrophils (mean ± SD, $n = 3$ wells from one experiment representative of three). Drug-treated (and untreated) neutrophils were also exposed to an fMLP gradient generated by addition of 100 nM fMLP (1 μL) in the EZ-TAXIScan device. Images and cell tracks of migrating neutrophils were evaluated for directionality, upward directionality and percentage of neutrophils displaying multiple pseudopodia as described earlier ($n = 20$ cells; *$P < 0.05$). (*E*) H_20_2 treatment of NADPH oxidase–inhibited human neutrophils rescues defect in pseudopod formation and chemotaxis. Human neutrophils were pretreated with 50 μM DPI (or without) and then treated with (or without) 100 μM H_20_2 for 5 min and then allowed to chemotax in response to a fMLP gradient in the EZ-TAXIScan device as described earlier. Migrating neutrophils were evaluated ($n = 20$ cells; *$P < 0.05$ vs. DPI-treated neutrophils) for directionality, upward directionality, and percentage of neutrophils displaying multiple pseudopodia as described earlier.

We focused on the 12 compounds that led to impaired directionality, but did not inhibit neutrophil migration completely (Figs. S2 and S3). Five of these drugs are compounds that inhibit microtubule polymerization, which is consistent with recent reports indicating that microtubules negatively regulate uropod signaling and enhance directional sensing in neutrophils (10, 11). Interestingly, the most dramatic inhibitory effect was induced by diphenyleneiodonium chloride (DPI), a well characterized and commonly used flavoprotein inhibitor that was known to suppress activity of NADPH oxidase and NOS (12–14). As neutrophil chemotaxis was not affected by other NOS inhibitors (e.g., 7-nitroindazole, L-NIO dihydrochloride, 1-[2-(trifluoromethyl) phenyl]imidazole, 2-amino-5,6-dihydro-6-methyl-4H-1,3 thiazine, ethylisothiourea, S-isopropylisothiourea hydrobromide, NG-methyl-L-arginine, nω-nitro-l-arginine methyl ester, nω-nitro-L-arginine, and L-canavanine) or NO donors (3-morpholinosydnonimine, s-nitrosoglutathione, and spermine NONOate; Dataset S1), it is most likely that the effect of DPI on neutrophil chemotaxis was mediated by the inhibition of NADPH oxidase, suggesting that chemoattractant elicited ROS production might play a role in regulating neutrophil chemotactic migration.

ROS Are Physiological Regulators of Neutrophil Chemotactic Migration. We further investigated the effect of DPI on neutrophil directional migration using a transwell migration system. Cells were plated on transwell filters and induced to migrate in response to

chemoattractant added to wells beneath the filters. The migration of neutrophils to these lower wells requires 2D chemotaxis on top of the filter (toward the holes), followed by migration through the holes into the bottom well of chemoattractant. The number of cells in the bottom well was then used to calculate percentage of cells migrated. Consistent with the EZ-TAXIScan results, treatment with DPI significantly inhibited neutrophil migration into the lower wells (Fig. 1*A*). To take a closer look at the morphological changes elicited by DPI treatment, multiple pseudopod formation was measured in chemotaxing neutrophils. We observed that DPI-treated neutrophils showed multiple pseudopodia much more frequently compared with untreated neutrophils, although the migration speed of these two populations was essentially the same (Fig. 1*B*). The DPI-induced inhibitory effect appeared not to be specific to chemotaxis-elicited by chemoattractant N-formyl-methionyl-leucyl-phenylalanine (fMLP), which was used for the initial screening. Treatment with DPI also significantly inhibited chemotaxis elicited by leukotriene B4 (LTB4) and IL-8, suggesting that DPI might block a general pathway in directional migration (Fig. 1*C*). Interestingly, IL-8–mediated chemotaxis was more resistant to DPI treatment compared with fMLP and LTB4. It seems that this is not a sensitivity

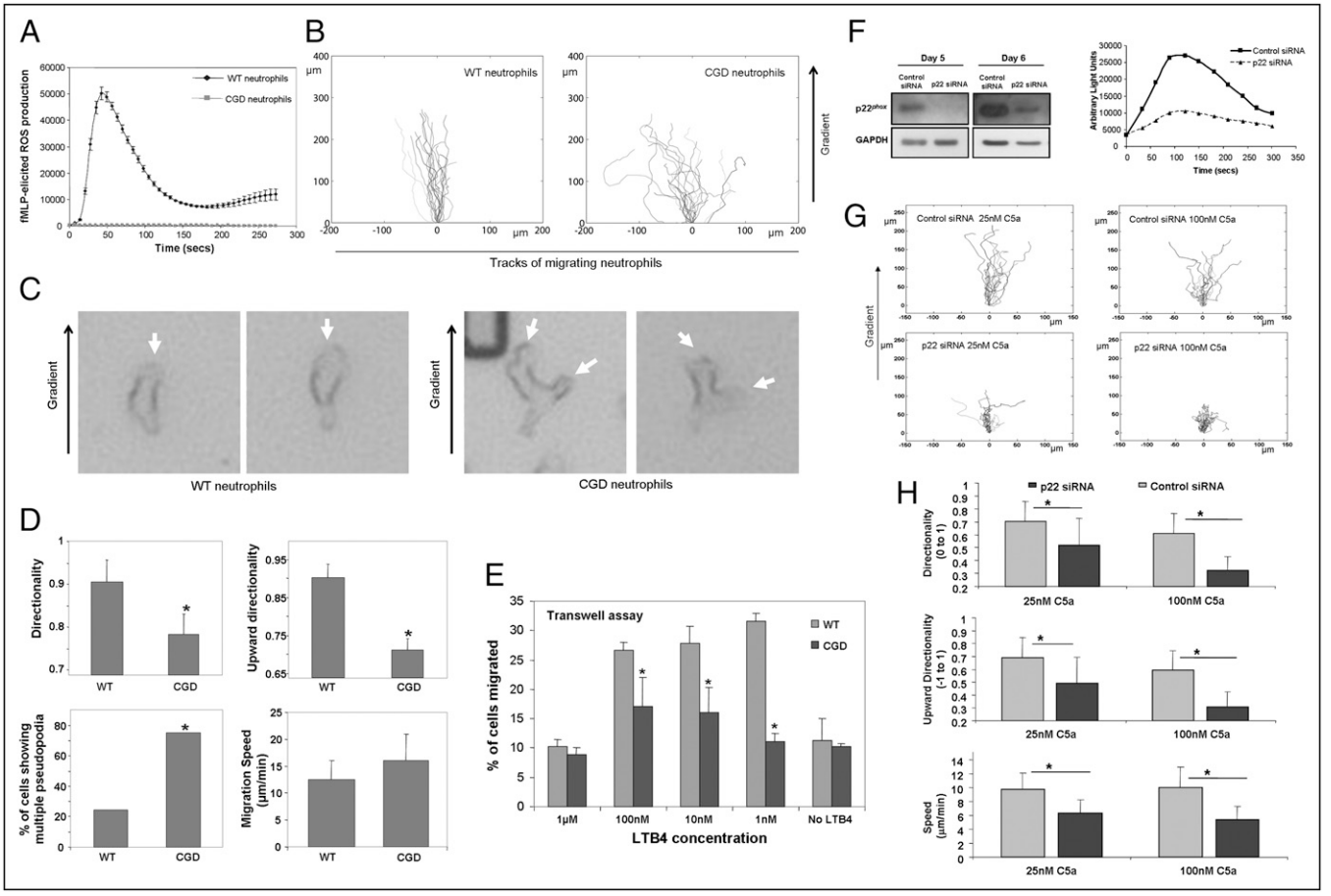

Fig. 2. Disruption of NADPH oxidase leads to chemotaxis defects. (*A*–*E*) Neutrophils from CGD mice do not produce ROS in response to chemoattractant stimulation, display multiple pseudopodia, and show loss of directionality during chemotaxis. (*A*) ROS production in neutrophils (5×10^5) from WT or CGD mice after stimulation with 1 μM fMLP was evaluated by monitoring chemiluminescence (for 1 s) every 7 s for 280 s, in the presence of 50 μM luminol and 0.8 U HRP in a luminometer at 37 °C. Data represents mean ± SD from three wells from one experiment representative of three. (*B*) Neutrophils from WT and CGD mice (3,000 cells) were plated into the EZ-TAXIScan device and exposed to a shallow chemoattractant gradient generated by addition of 1 μL LTB4 (100 nM). Cell tracks of migrating WT (*Left*) and CGD (*Right*) neutrophils (cells that move ≥65 μm from the bottom of the channel; $n = 20$) were traced from captured images, realigned such that all cells started from the same starting point (0,0) and plotted. Chemoattractant concentration increases in the positive y direction. (*C*) Representative images of WT (*Left*) and CGD migrating neutrophils (*Right*) are also shown; white arrowheads specify pseudopodia. (*D*) Migrating neutrophils were evaluated ($n = 20$ cells; $^*P < 0.05$ vs. WT neutrophils) for directionality, upward directionality, percentage of neutrophils displaying multiple pseudopodia, and migration speed as described earlier. (*E*) Transwell migration of CGD mice neutrophils. WT or CGD murine neutrophils were allowed to migrate in response to the indicated concentration of LTB4. Percentage of cells that migrated into the bottom well was recorded. Data shown are means ± SD from three wells from one experiment representative of three. ($^*P < 0.05$ vs. WT neutrophils.) (*F*–*H*) Knocking down p22phox via siRNA results in impaired cell migration and chemotaxis. HL60 cells were differentiated with 1.75% DMSO for 1 d, transfected with 1 μM control siRNA or p22phox siRNA, and further differentiated until d 5 or 6. (*F*) Knockdown of p22phox in dHL60 cells. At d 5 (*Left*) or d 6 (*Right*), dHL60 cells were lysed and probed with p22phox antibody to evaluate knockdown and GAPDH antibody to evaluate loading. (*G*) Decreased ROS production in p22phox-knockdown dHL60 cells. ROS production in control siRNA or p22phox siRNA transfected dHL60 cells (2×10^5, 5 d of differentiation) after stimulation with 10 nM C5a was evaluated by monitoring chemiluminescence (for 1 s) every 30 s for 300 s, in the presence of 50 μM luminol and 0.8 U HRP in a luminometer at 37 °C. (*H*) Control siRNA or p22phox siRNA transfected dHL60 cells (d 5) were exposed to a chemoattractant gradient generated by addition of 25 nM or 100 nM C5a (1 μL) in the EZ-TAXIScan device and imaged every 0.5 min for 20 min. Cell tracks of migrating dHL60 cells ($n = 15$) were traced from the captured images, realigned to start from the same point (0,0), and plotted (*Left*). Migration paths of the dHL60 cells were evaluated for a 0- to 20-min time frame ($n > 15$ cells, $^*P < 0.005$ vs. control siRNA dHL60 cells) for directionality, upward directionality, and migration speed as described in *Experimental Procedures* (*Right*).

issue, as we checked several chemoattractant concentrations and the effect of DPI treatment on IL-8–induced chemotaxis is always weaker (Fig. S4). This effect might be caused by relatively lower ROS production in IL-8–treated cells. Chemical inhibitors often have multiple targets. DPI may also inhibit other flavin-containing enzymes. To ensure that the DPI-induced neutrophil chemotaxis defect was indeed caused by inhibition of NADPH oxidase, we examined another NADPH oxidase inhibitor, sinomenine (15). Similar to DPI, sinomenine induced multiple pseudopodia in chemotaxing neutrophils and significantly reduced chemotaxis efficiency. Interestingly, two of the compounds identified from the initial screening, EHNA hydrochloride and LE135, previously known as adenosine deaminase inhibitor and retinoic acid antagonist, respectively, also drastically suppressed chemoattractant-elicited NADPH oxidase activation, again indicating the involvement of ROS in chemotactic migration (Fig. 1*D* and Fig. S5). Further supporting this hypothesis is the observation that DPI-induced chemotaxis defects were partially rescued by including H_2O_2 in chemotaxis buffer (Fig. 1*E*).

NADPH Oxidase Is Required for Efficient Neutrophil Chemotaxis. Although DPI is a well known and commonly used NADPH oxidase, its effect on cell migration may be mediated by other undefined mechanisms. To definitely prove that the DPI-induced neutrophil chemotaxis defect is at least partially caused by inhibition of NADPH oxidase, we next explored neutrophil chemotaxis using a CGD mouse in which gp91 subunit of NADPH oxidase holoenzyme was deleted and thus chemoattractant-elicited superoxide production was completely abolished (Fig. 2*A*). Similar to chemical inhibition, neutrophils isolated from these mice displayed multiple pseudopods (Fig. 2*C*) and reduced chemotaxis efficiency (Fig. 2 *B* and *D*). Consistently, neutrophils isolated from the CGD mice also displayed a migration defect in the transwell assay compared with WT neutrophils (Fig. 2*E*). Finally, we investigated the chemotaxis of neutrophil-like differential HL60 cells in which the $p22^{phox}$ subunit of NADPH oxidase was knocked down by a specific siRNA, and essentially the same results were observed (Fig. 2 *F–H*). Collectively, all these results suggest that signal-induced NADPH oxidase-mediated ROS production plays an essential role in regulating neutrophil chemotaxis.

Neutrophils Isolated from CGD Patients Also Show Severe Chemotaxis Defect. To further explore the physiological and clinical significance of the regulation of neutrophil migration by ROS, we examined chemotaxis behaviors of neutrophils isolated from a CGD patient that contain mutated alleles of the gene encoding $gp91^{phox}$. As expected, neutrophils from the CGD patient displayed impaired chemoattractant-elicited ROS production in comparison with neutrophils from a healthy volunteer (Fig. 3*A*). The ROS peak in these neutrophils is significant, but is much smaller than that in the WT neutrophils. Adhesion-induced ROS production in the absence of chemoattractant was also abolished in the CGD neutrophils. The CGD neutrophils displayed a striking chemotaxis defect, showing lack of directionality, more frequent formation of multiple pseudopodia, and slow migration toward the direction of higher chemoattractant (Fig. 3*B*). It is noteworthy that the CGD patient in this study was receiving IFN-γ treatment. Nevertheless, it is unlikely that the observed neutrophil chemotaxis defect was a result of this treatment, as IFN-γ–treated WT neutrophils showed normal directionality during chemotaxis. Collectively, these results suggest that the defective neutrophil chemotaxis might be contributive to the compromised bactericidal activity in CGD patients, providing a cellular mechanism for CGD pathogenesis.

CGD Mice Display Impaired in Vivo Neutrophil Recruitment. Our in vitro experiments showed that neutrophils depleted of ROS display reduced chemotaxis efficiency. We next investigated whether this

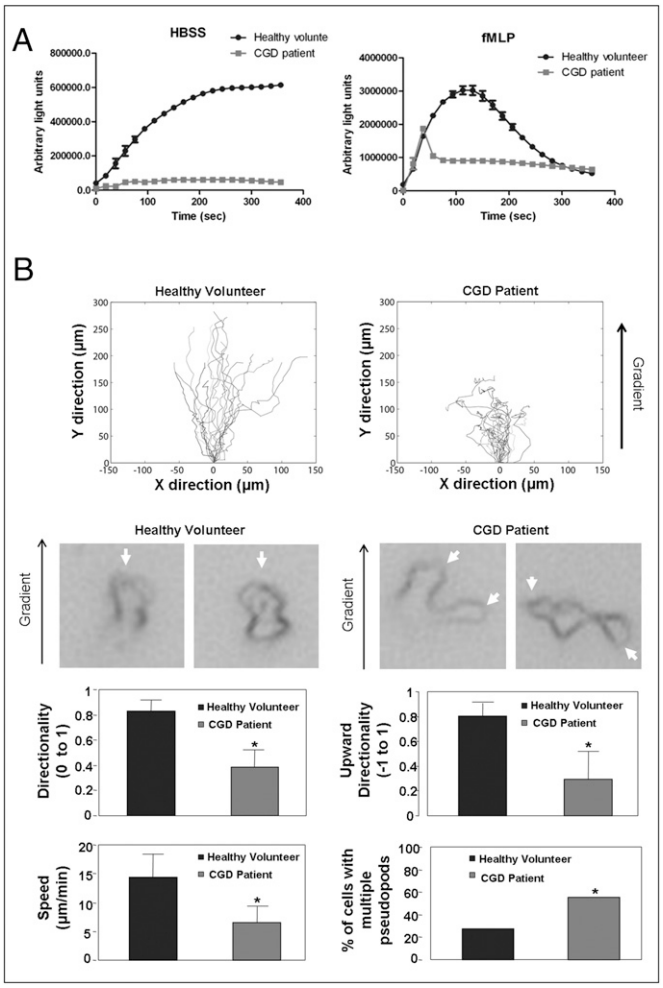

Fig. 3. Neutrophils isolated from the CGD patient are defective in ROS production and chemotactic migration. (*A*) Decreased ROS production in neutrophils from a CGD patient. ROS production in neutrophils (5×10^5) from a CGD patient or a healthy volunteer after addition of HBSS (*Top*) or 100 nM fMLP (*Bottom*) was evaluated by monitoring chemiluminescence (for 1 s) every 20 s for 360 s, in the presence of 50 μM isoluminol and 0.8 U HRP in a luminometer at 37 °C. Data represent mean ± SD from three wells. (*B*) Neutrophils from the CGD patient or healthy volunteer were exposed to a chemoattractant gradient generated by addition of 100 nM fMLP (1 μL) in the EZ-TAXIScan device and imaged every 0.5 min for 20 min. Cell tracks of migrating neutrophils (n = 20) were traced from the captured images, realigned to start from the same point (0,0), and plotted (*Top*). Images of chemotaxing neutrophils from the CGD patient or healthy volunteer are shown (*Middle*). White arrowheads specify pseudopodia in the cells. Neutrophils were evaluated (n = 20 cells, $^*P < 0.01$ vs. WT neutrophils) for directionality, upward directionality, percentage of neutrophils displaying multiple pseudopodia, and migration speed as described earlier (*Bottom*).

defect in chemotaxis will lead to impaired neutrophil recruitment to sites of inflammation in live mice using a murine acute peritoneal inflammation (i.e., peritonitis) model. To compare neutrophil recruitment under exactly the same environment, an adoptive transfer experiment was conducted (Fig. S6). We labeled in vitro purified CGD neutrophils with intracellular fluorescent dye 5- (and 6-) carboxyfluorescein diacetate succinimidyl esters (CFSE; green) and WT neutrophils with another dye, 5- (and 6-) chloromethyl SNARF-1 acetate (red), or vice versa. The mixed (1:1) population was i.v. injected into a WT recipient mouse 2.5 h after the i.p. thioglycolate (TG) injection. By doing this, variability caused by difference in inflammatory environment in each individual recipient mouse will be eliminated. CGD (green) and WT (red) neutrophils

CELL BIOLOGY

were identified by their unique fluorescent labels. As we measured neutrophil numbers at 4 h after the TG injection, when neutrophil death is minimal, the ratio of CGD neutrophils to WT neutrophils most likely reflected their relative capability to migrate to the inflamed peritoneal cavity. Consistent with the in vitro results, we detected a much reduced peritoneal recruitment of CGD neutrophils compared with WT neutrophils (Fig. 4*A*). A similar effect was also detected in a murine air pouch model in which recruitment of adoptively transferred neutrophils to a preformed air pouch was induced by TNF-α (Fig. 4*B*). These results further support the conclusion that ROS generated by NADPH oxidase are key physiological regulators of actin dynamics in neutrophils.

Discussion

In this study, using an unbiased screening approach, we have identified ROSs as essential players for modulating neutrophil chemotaxis. Chemotaxis is a process in which cells sense and move up a gradient of molecules (chemoattractants). It plays a central role in the regulation of host defense and inflammatory reactions by recruiting circulating effector leukocytes, including neutrophils, monocytes, and effector T cells, to the sites of injury or infection. During chemotaxis, chemoattractants elicit a number of changes in neutrophils. These include a localized polymerization of F-actin at the site of cell cortex closest to the chemoattractant source, a morphological change characterized by cell elongation, the formation of new lamellipodia or pseudopods at the leading edge, and the forward protrusion of the leading edge followed by retraction of posterior of the cell. We have found that neutrophils with inhibited ROS production that were isolated from CGD patients or mice or pharmacologically/siRNA–treated to inhibit the NADPH oxidase complex displayed defective migration. These neutrophils formed more frequent multiple pseudopodia and lost their directionality as they migrated up a chemoattractant concentration gradient.

CGD is an inherited disorder characterized by recurrent bouts of infection as well as chronic inflammation with granuloma formation. Consistently, neutrophil recruitment to sites of inflammation is dramatically elevated in the CGD mice (16). This hyperinflammatory phenotype is likely caused by dysfunctional kynurenine pathway of tryptophan catabolism (17) and suppression of ROS-induced deactivation of proinflammatory chemokines such as C5a, fMLP (18), LTB4 (19), and IL8 (20). At the sites of infection, the inability of CGD neutrophils to produce ROS in response to chemoattractant stimulation may contribute to the impaired bactericidal activity of these cells. Our discovery that depletion of signal-elicited ROS production in fact inhibits neutrophil chemotactic migration provides another cellular mechanism for CGD pathogenesis and might lead to development of new therapeutic strategies for this disease.

How is chemotactic migration regulated by ROSs? ROSs have been identified as important second messengers that can regulate intracellular signal transduction under a variety of physiological and pathophysiological conditions. This has been shown to occur predominantly via oxidation of thiols (-SH) on protein cysteine

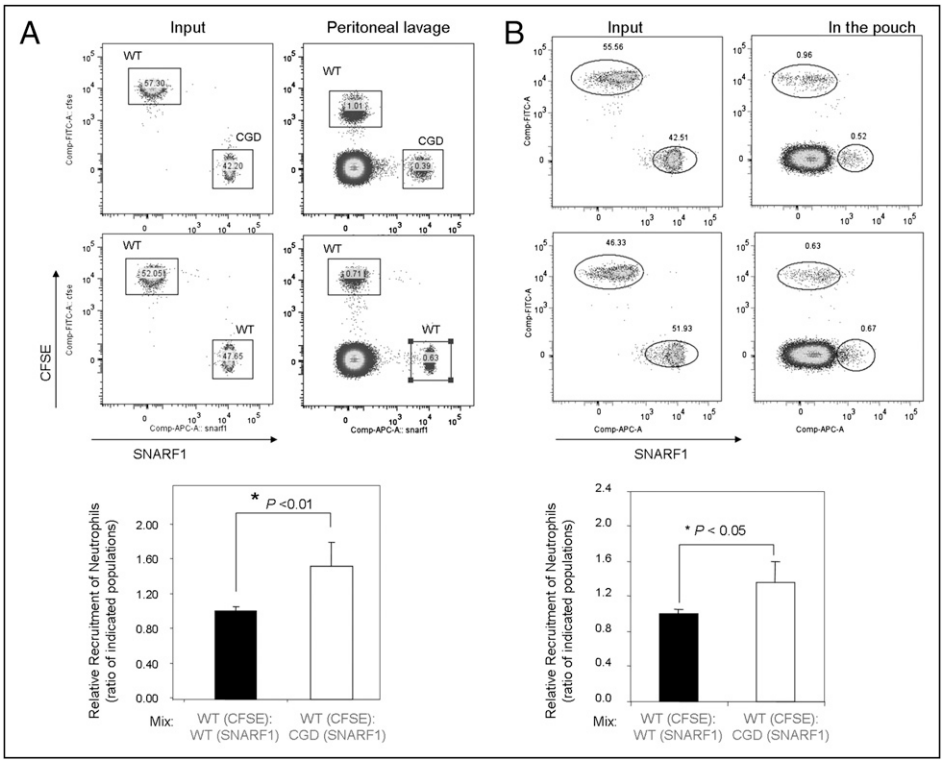

Fig. 4. CGD neutrophils exhibit an intrinsic defect in recruitment to sites of inflammation. (*A*) Recruitment of adoptively transferred neutrophils in the TG-induced peritonitis model. Neutrophils isolated from WT and CGD mice were labeled with intracellular fluorescent dye CFSE (final concentration, 1 μM; Molecular Probes) or 5- (and 6-) chloromethyl SNARF-1 acetate (final concentration, 1 μM; Molecular Probes) at 37 °C for 10 min. Labeled cells were mixed (1:1) as indicated and then injected i.v. (via tail vein) into WT mice that have been challenged with 1 mL 3% TG for 2.5 h. Peritoneal fluids were harvested 1.5 h after the injection of cell mixture. The amount of adoptively transferred neutrophils recruited to the peritoneal cavity was analyzed using a BD FACSCanto II flow cytometer (Becton Dickinson) and BD FACSDiva software. Relative recruitment of neutrophil was calculated as the ratio of indicated populations in the peritoneal cavity. (*B*) Recruitment of adoptively transferred neutrophils to a preformed air pouch. The dorsal air pouch was generated on WT recipient mice as described in *Experimental Procedures*. Neutrophil recruitment to the pouch was induced by TNF-α, which was directly injected into the pouch 2.5 h before the neutrophil injection. The pouch was flushed 1.5 h after the injection of cell mixture. The relative recruitment of WT and CGD neutrophil was calculated as described earlier.

residues, resulting in reversible protein posttranslational modifications such as glutathionylation, disulfide bond formation, and sulfenic acid formation. Many of these modifications control signal transduction by altering functionality/activity of the protein involved. Redox regulation of numerous proteins such as Ras, protein tyrosine kinases (Src kinases), and protein tyrosine phosphatases have been reported and are known to alter protein functions. PTEN has also been identified as a target of ROSs (21–23). ROSs can also directly regulate actin polymerization via modifying G-actin monomers (21–23). In addition, the NADPH oxidase is also essential for chemoattractant-elicited depolarization of membrane potential and can regulate Ca^{2+}, K^{+} homeostasis in neutrophils (24). This may contribute to directional sensing in an indirect way. The exact mechanism by which ROS regulate neutrophil chemotaxis needs to be further investigated. During chemotaxis, many signaling events take place locally within the cell. For example, Rac-related signaling and actin polymerization are detected at the leading edge of chemotaxing cells, whereas RhoA activation and contractile actin–myosin complexes appear only at the back of the cells. Interestingly, we found NADPH oxidase was highly enriched near the leading edge of migrating neutrophils (Fig. S7). Whether this specific localization is essential for chemotaxis needs to be further investigated.

Experimental Procedures

Neutrophil Purification and Functional Assays. Human blood neutrophil purification, murine bone marrow neutrophil purification, quantification of F-actin levels by phalloidin labeling, measurement of superoxide production by luminol chemiluminescence, micropipette chemotaxis, and transwell migration assays were performed as described previously (25–27). Peripheral blood was obtained from a human CGD patient and healthy volunteer, with informed consent. EZ-TAXIScan chemotaxis assay, analysis of cell tracks and morphology, siRNA knockdown, and other related assays are described in *SI Materials and Methods*.

Recruitment of Adoptively Transferred Neutrophils in TG-Induced Peritonitis. Peritonitis was induced as previously described (26). Neutrophils isolated from WT and CGD mice were labeled with intracellular fluorescent dye CFSE (final concentration, 1 μM; Molecular Probes) or 5- (and 6-) chloromethyl SNARF-1 acetate (final concentration, 1 μM; Molecular Probes) at 37 °C for 10 min. Labeled cells were mixed as indicated in Fig. S6 then injected i.v. (via tail vein) into WT mice that have been challenged with 1 mL 3% TG for 2.5 h. Mice were euthanized by CO_2 inhalation 1.5 h after the injection of cell mixture (4 h after TG injection) and peritoneal exudate cells were recovered by peritoneal lavage with 10 mL of ice-cold PBS solution containing 5 mM EDTA. The amount of adoptively transferred neutrophils recruited to the peritoneal cavity was analyzed using a BD FACSCanto II flow cytometer (Becton Dickinson) and BD FACSDiva software. Relative recruitment of neutrophil was calculated as the ratio of indicated populations in the peritoneal cavity.

Recruitment of Adoptively Transferred Neutrophils in a Murine Dorsal Air Pouch Model. A dorsal air pouch was created by injecting mice with 5 mL of air s.c. on the back at d 0. On d 3 and 5, the pouches were reinflated with 2 mL of air. At 6 d after the initial air injection, TNF-α (in 0.5 mL sterile 0.9% saline solution) was directly injected into the pouch. Four hours after TNF-α injection, mice were anesthetized, and the pouch was flushed with 2 mL saline solution. The relative recruitment of WT and CGD neutrophils was calculated as described earlier.

Statistics. Analysis of statistical significance for indicated data sets was performed using the Student *t* test capability on Microsoft Excel.

ACKNOWLEDGMENTS. The authors thank Leslie Silberstein, John Manis, Li Cai, and Narayanaswamy Ramesh for helpful discussions; and Dan Stevens from Hirata Corp for assistance with the EZ-TAXIScan device. B.S. was supported by National Institutes of Health (NIH) training Grant HL066987. H. L. was supported by NIH Grants HL085100, AI076471, HL092020, and GM076084, and a Research Scholar Grant from the American Cancer Society.

1. Iijima M, Devreotes P (2002) Tumor suppressor PTEN mediates sensing of chemoattractant gradients. *Cell* 109:599–610.
2. Funamoto S, Meili R, Lee S, Parry L, Firtel RA (2002) Spatial and temporal regulation of 3-phosphoinositides by PI 3-kinase and PTEN mediates chemotaxis. *Cell* 109:611–623.
3. Li Z, et al. (2005) Regulation of PTEN by Rho small GTPases. *Nat Cell Biol* 7:399–404.
4. Li Z, et al. (2003) Directional sensing requires G beta gamma-mediated PAK1 and PIX alpha-dependent activation of Cdc42. *Cell* 114:215–227.
5. Chodniewicz D, Zhelev DV (2003) Chemoattractant receptor-stimulated F-actin polymerization in the human neutrophil is signaled by 2 distinct pathways. *Blood* 101: 1181–1184.
6. Andrew N, Insall RH (2007) Chemotaxis in shallow gradients is mediated independently of PtdIns 3-kinase by biased choices between random protrusions. *Nat Cell Biol* 9: 193–200.
7. Chen L, et al. (2003) Two phases of actin polymerization display different dependencies on PI(3,4,5)P3 accumulation and have unique roles during chemotaxis. *Mol Biol Cell* 14: 5028–5037.
8. Loovers HM, et al. (2006) Distinct roles of PI(3,4,5)P3 during chemoattractant signaling in Dictyostelium: a quantitative in vivo analysis by inhibition of PI3-kinase. *Mol Biol Cell* 17:1503–1513.
9. Chen L, et al. (2007) PLA2 and PI3K/PTEN pathways act in parallel to mediate chemotaxis. *Dev Cell* 12:603–614.
10. Xu J, Wang F, Van Keymeulen A, Rentel M, Bourne HR (2005) Neutrophil microtubules suppress polarity and enhance directional migration. *Proc Natl Acad Sci USA* 102: 6884–6889.
11. Niggli V (2003) Microtubule-disruption-induced and chemotactic-peptide-induced migration of human neutrophils: implications for differential sets of signalling pathways. *J Cell Sci* 116:813–822.
12. Stuehr DJ, et al. (1991) Inhibition of macrophage and endothelial cell nitric oxide synthase by diphenyleneiodonium and its analogs. *FASEB J* 5:98–103.
13. Cross AR, Jones OT (1986) The effect of the inhibitor diphenylene iodonium on the superoxide-generating system of neutrophils. Specific labelling of a component polypeptide of the oxidase. *Biochem J* 237:111–116.
14. Ellis JA, Cross AR, Jones OT (1989) Studies on the electron-transfer mechanism of the human neutrophil NADPH oxidase. *Biochem J* 262:575–579.
15. Qian L, et al. (2007) Sinomenine, a natural dextrorotatory morphinan analog, is anti-inflammatory and neuroprotective through inhibition of microglial NADPH oxidase. *J Neuroinflammation* 4:23.
16. Pollock JD, et al. (1995) Mouse model of X-linked chronic granulomatous disease, an inherited defect in phagocyte superoxide production. *Nat Genet* 9:202–209.
17. Romani L, et al. (2008) Defective tryptophan catabolism underlies inflammation in mouse chronic granulomatous disease. *Nature* 451:211–215.
18. Clark RA, Klebanoff SJ (1979) Chemotactic factor inactivation by the myeloperoxidase-hydrogen peroxide-halide system. *J Clin Invest* 64:913–920.
19. Segal BH, Kuhns DB, Ding L, Gallin JI, Holland SM (2002) Thioglycollate peritonitis in mice lacking C5, 5-lipoxygenase, or p47(phox): complement, leukotrienes, and reactive oxidants in acute inflammation. *J Leukoc Biol* 71:410–416.
20. Lekstrom-Himes JA, Kuhns DB, Alvord WG, Gallin JI (2005) Inhibition of human neutrophil IL-8 production by hydrogen peroxide and dysregulation in chronic granulomatous disease. *J Immunol* 174:411–417.
21. Rhee SG (2006) Cell signaling. H2O2, a necessary evil for cell signaling. *Science* 312: 1882–1883.
22. Clavreul N, et al. (2006) S-glutathiolation of p21ras by peroxynitrite mediates endothelial insulin resistance caused by oxidized low-density lipoprotein. *Arterioscler Thromb Vasc Biol* 26:2454–2461.
23. Shelton MD, Chock PB, Mieyal JJ (2005) Glutaredoxin: role in reversible protein s-glutathionylation and regulation of redox signal transduction and protein translocation. *Antioxid Redox Signal* 7:348–366.
24. Rada BK, Geiszt M, Hably C, Ligeti E (2005) Consequences of the electrogenic function of the phagocytic NADPH oxidase. *Philos Trans R Soc Lond B Biol Sci* 360:2293–2300.
25. Zhu D, et al. (2006) Deactivation of phosphatidylinositol 3,4,5-trisphosphate/Akt signaling mediates neutrophil spontaneous death. *Proc Natl Acad Sci USA* 103: 14836–14841.
26. Subramanian KK, et al. (2007) Tumor suppressor PTEN is a physiologic suppressor of chemoattractant-mediated neutrophil functions. *Blood* 109:4028–4037.
27. Jia Y, et al. (2007) Inositol 1,3,4,5-tetrakisphosphate negatively regulates phosphatidylinositol-3,4,5- trisphosphate signaling in neutrophils. *Immunity* 27:453–467.

Supporting Information

Hattori et al. 10.1073/pnas.0914351107

SI Methods

Analysis of Cell Tracks and Morphology. *(x,y)* coordinates of migrating neutrophils (i.e., neutrophils that cross >65 μm from the starting line) were tracked from sequential images using DIAS imaging software (Solltech). Cell tracks were then realigned such that all of the cells started from the same starting point (0,0) and plotted using Matlab. Migration parameters are described in detail in Fig. S3. Directionality and upward directionality were calculated as the straight-line migration distance from the origin divided by total migration length and straight-line distance migrated in the upward direction divided by total migration length (Fig. S3). Migration speed (in μm/min) was calculated as average of cell speeds (migration distance between the current frame and the previous frame divided by the time between sequential frames, 0.5 min) at each captured frame. All parameters were calculated only for migrating cells in the 5 min to 15 min time frame of each movie. Percentage of neutrophils with multiple pseudopodia during the course of the 20-min video was evaluated from images of migrating cells. Fisher exact test (2 × 2) was performed to evaluate significant difference from untreated or WT neutrophils.

EZ-TAXIScan Chemotaxis Assay. The EZ-TAXIScan chamber (Effector Cell Institute) was assembled with a 260-μm-wide × 4-μm-thick silicon chip on a 2-mm untreated glass base, as described by the manufacturer and filled with RPMI/0.1% BSA. Inhibitor-treated (or carrier-treated) neutrophils (1 μL, 3×10^6/mL) were added to the lower reservoir of each of the six channels and allowed to line up by removing 18 μL of buffer from the upper reservoir. RPMI/0.1% BSA (15 μL with the appropriate pharmacological inhibitor) was then added to fill both reservoirs to the brim. One microliter of chemoattractant (fMLP, C5a, or LTB4) was then added to the upper reservoir and neutrophil migration (at 37 °C) in each of the channels was captured sequentially every 30 s for 20 min using a 10× lens on a Discovery Screening System (Universal Imaging). Pharmacological inhibitors (from Tocris Bioscience library) along with 200 nM of pan-PI3K inhibitor wortmannin (used to reduce random migration) were added directly to human neutrophils (100 μL, 3×10^6/mL) in RPMI/0.1% BSA and incubated in a 37 °C, 5% CO_2 chamber for 30 min before the chemotaxis assay.

CGD Mice. X-linked CGD mice (1) that contain disrupted alleles of the gene encoding gp91^{phox} (B6.129S6-Cybbtm1Din/J; strain, C57BL/6) were purchased from Jackson Laboratories. In all of the experiments performed with the CDG mice, we used C57BL/6 mice of the same age as WT controls. All procedures involving mice were approved and monitored by the Animal Care and Use Committee of Children's Hospital Boston.

Knockdown of p22^{phox} A predesigned duplexed Stealth siRNA (Invitrogen) that targets p22^{phox} (CYBA gene; accession no., NM_000101.2) was used to knock down p22^{phox} in dHL60 cells (sense sequence, ACU AUG UUC GGG CCG UCC UGC AUC U; antisense sequence, AGA UGC AGG ACG GCC CGA ACA UAG U). The negative control used was an ON-TARGETplus nontargeting siRNA 2 (Dharmacon). For gene silencing HL60 cells were differentiated for 1 d with 1.75% DMSO. On d 1, 2×10^6 cells were resuspended in 100 μL Cell Line V nucleofector solution, mixed with 1 μM siRNA (negative control or p22^{phox}), and nucelofected using the T-019 program as per manufacturer instructions. Cells were then cultured in 2 mL IMDM plus 20% FBS plus 1.75% DMSO for 4 to 5 d, and then harvested for Western blotting, ROS production, and chemotaxis assays. Lysates of differentiated HL60 cells were probed for p22^{phox} expression using an anti-rabbit p22^{phox} antibody (Santa Cruz Biotechnology) and loading was evaluated using a GAPDH antibody (Encor Biotechnology). ROS production assays and EZ-TAXIScan chemotaxis assays were performed as described earlier.

1. Pollock JD, et al. (1995) Mouse model of X-linked chronic granulomatous disease, an inherited defect in phagocyte superoxide production. *Nat Genet* 9:202–209.

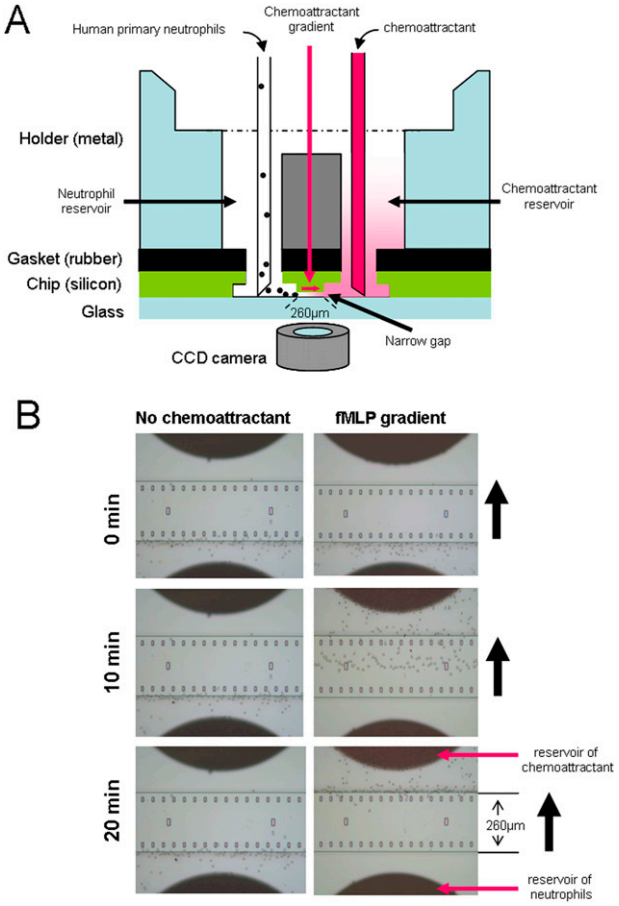

Fig. S1. Screening for pharmacological agents that modulate actin dynamics during neutrophil chemotaxis. (*A*) Cross-sectional schematic view of one of the six channels in EZ-TAXIScan device. The apparatus consists of a six-channel silicon chip (with two holes for each channel) pressed on top of a glass surface using a rubber gasket and metal holder. Cells (1 μL) are loaded to the bottom of one reservoir and chemoattractant (1 μL) is added to the other reservoir. This sets up a chemoattractant gradient between the reservoirs, driving cells to migrate toward the chemoattractant reservoir through a narrow gap (4 μm height, 260 μm length) between the silicon chip and glass surface. Images of migrating cells in each of the six channels are captured in parallel using a 10× lens coupled to a CCD camera. (*B*) Chemotaxis of human neutrophils in response to chemoattractant fMLP. Human neutrophils (3,000 cells) were plated into the neutrophil reservoir (bottom well) of the EZ-TAXIScan device and exposed to no chemoattractant (*Left*) or to a chemoattractant gradient (*Right*) generated by addition of 100 nM fMLP (1 μL) into the chemoattractant reservoir (top well). Images of neutrophils are shown at 0 min, 10 min, and 20 min after chemoattractant addition.

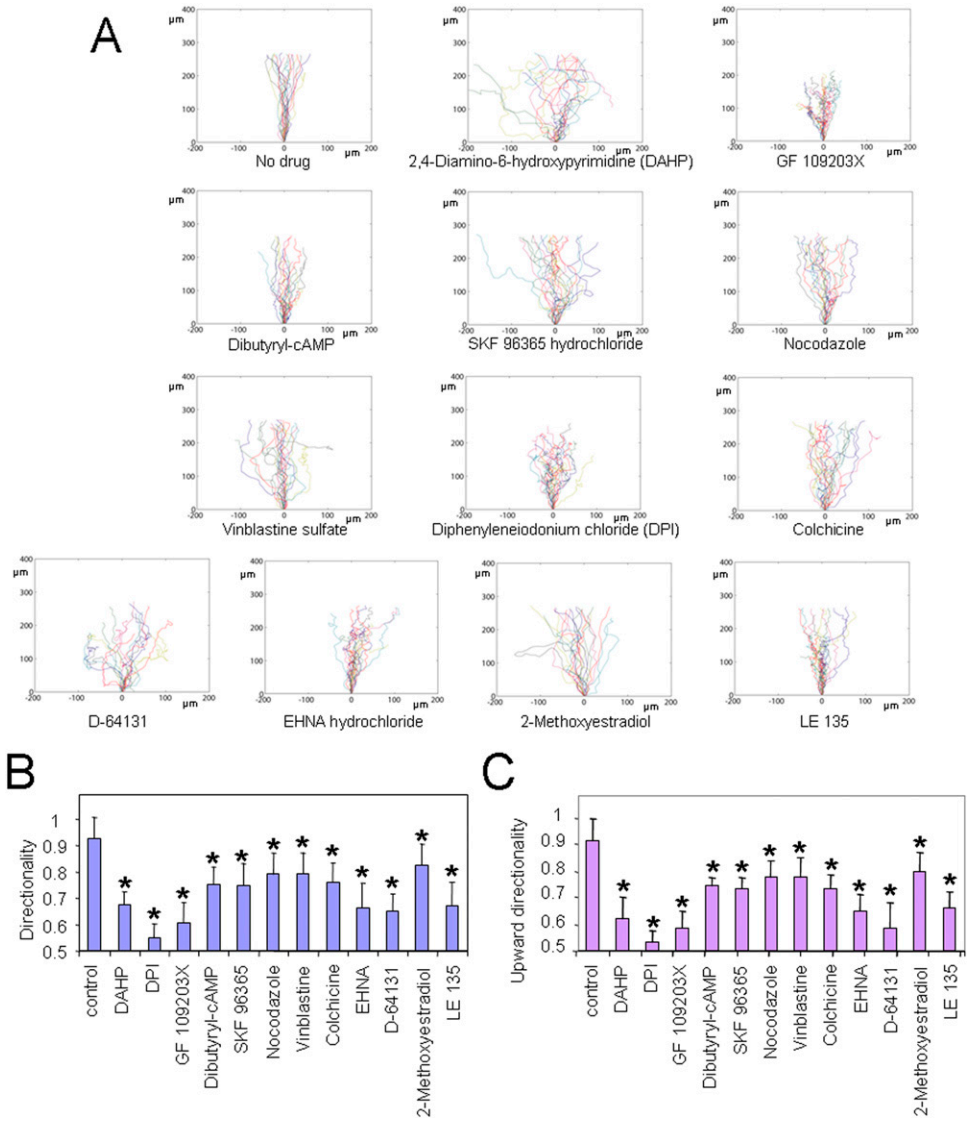

Fig. S2. Biologically active pharmacological agents that decrease chemotaxis efficiency of human neutrophils. Neutrophils were incubated at 37 °C for 30 min without any treatment or with the following pharmacological agents: 2,4-diamino-6-hydroxypyrimidine (DAHP; 300 μM), GF 109203X (58 μM), dibutyryl-cAMP (1 mM), SKF 96365 hydrochloride (56 μM), nocodazole (16 μM), vinblastine sulfate (1.78 μM), DPI (100 μM), colchicine (10 μM), D-6413 (0.74 μM), EHNA hydrochloride (40 μM), 2-methoxyestradiol (19 μM), and LE 135 (14 μM). They were then exposed to a chemoattractant gradient generated by addition of 100 nM fMLP (1 μL) in the EZ-TAXIScan device and imaged every 0.5 min for 20 min. (*A*) Cell tracks of untreated and drug treated migrating neutrophils (cells that move ≥65 μm from the bottom of the channel; $n = 20$) were traced from the captured images, realigned such that all cells started from the same starting point (0,0), and plotted. Chemoattractant concentration increases in the positive y direction. (*B* and *C*) Cell tracks of migrating neutrophils in the 5 min to 15 min time frame were analyzed as described in *Experimental Procedures* to determine directionality (0–1) (*B*), defined as straight-line migration distance from the origin divided by the total migration length; and upward directionality (–1 to 1) (*C*), defined as straight-line distance migrated in the upward direction divided by total migration length (Fig. S3). Data in *B* and *C* are represented as mean ± SD for 20 cells. (*$P < 0.05$ versus untreated neutrophils.)

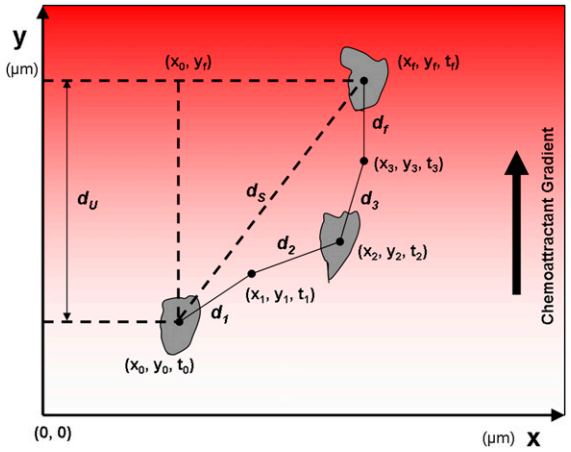

Fig. S3. Chemotaxis parameters for neutrophil migration in response to a chemoattractant gradient. If n is the number of successive frames analyzed and (xn, yn, tn) denotes the position of the neutrophil (xn, yn) at any time tn, the chemotaxis parameters can be calculated as follows: directionality (0–1) is dS / (d1 + d2 . . .+ df), speed (μm/min) is (d1 / (t1 − t0) + d2 / (t2 − t1) + . . .+ df / (tf − t3)) / n, and upward directionality (−1 to 1) is dU / (d1 + d2 . . .+ df). Here, "f" denotes the final position of the cell, "0" denotes the initial position, dn is the distance migrated between two successive frames (xn, yn) and (xn-1, yn-1), dS is the straight-line migration distance, i.e., distance between (x0, y0) and (xf, yf), and dU is the straight-line migration distance in the direction of the chemoattractant gradient (upward), i.e., distance between (x0, y0) and (x0, yf), yf-y0.

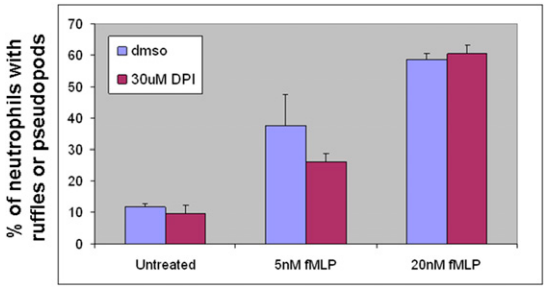

Fig. S4. Sensitivity to chemoattractant: Quantification of ruffling response and pseudopod formation. Murine neutrophils (0.5×10^4 cells in 50 μL) were pretreated with 30 μM DPI or not pretreated and then stimulated with 50 μL of 2× concentrated fMLP (or not stimulated) for 4 min. Cells were then fixed with 100 μL 4% formaldehyde in PBS solution, plated onto coverslips, and imaged. Percentage of neutrophils with ruffles or extended pseudopods were quantified from the images (1). More than 100 neutrophils were evaluated for each data point. Data are mean ± SD from three stimulations, from one experiment representative of three. ($P > 0.05$ vs. untreated.)

1. Subramanian KK, et al. (2007) Tumor suppressor PTEN is a physiologic suppressor of chemoattractant-mediated neutrophil functions. *Blood* 109:4028–4037.

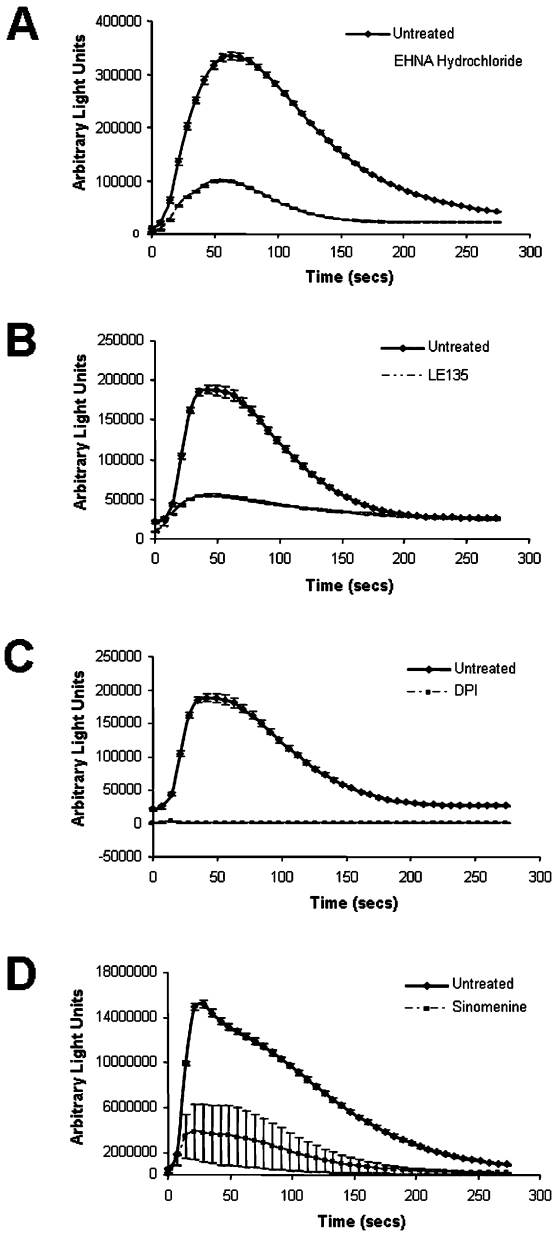

Fig. S5. Chemoattractant induced ROS production is suppressed by specific pharmacological inhibitors (raw data for Fig. 1*D* in the main text). Human blood neutrophils (5×10^5) were left untreated or treated with 40 μM EHNA hydrochloride (*A*), 14 μM LE 135 (*B*), 50 μM DPI (*C*), or 10 μM sinomenine (*D*) for 30 min at 37 °C. Cells were then stimulated with 100 nM fMLP, and ROS production was monitored in the presence of 50 μM luminol and 0.8 U of HRP in a luminometer at 37 °C. Chemiluminescence (in arbitrary light units) was recorded (for 1 sec) at indicated time points. Data are mean ± SD (n = 3) from one experiment representative of three. Assays for *A*–*D* were conducted on different days with blood neutrophils from different patients.

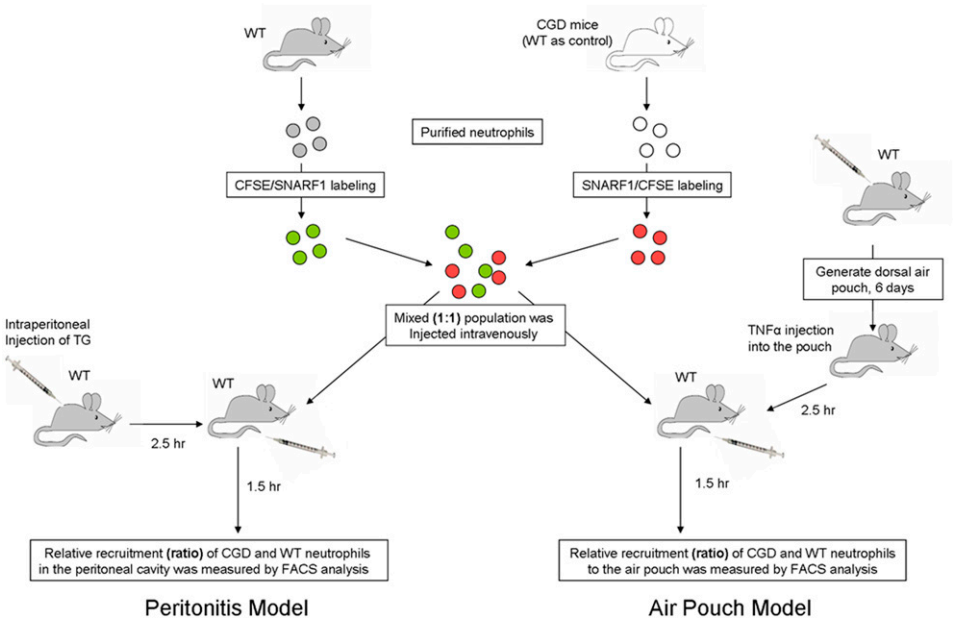

Fig. S6. Illustration of strategy used for adoptive transfer experiments. Bone marrow neutrophils from WT and CGD mice were labeled with different colors (SNARF1- or CFSE-labeled), mixed 1:1 and then i.v. injected into WT recipient mice that have been challenged with TG (intraperitoneally injected) or TNF-α (injected into an artificially generated dorsal air pouch). After 90 min, cells were collected from the peritoneal cavity or air pouch. The relative recruitment of CGD and WT neutrophils in the WT recipient was evaluated by FACS analysis.

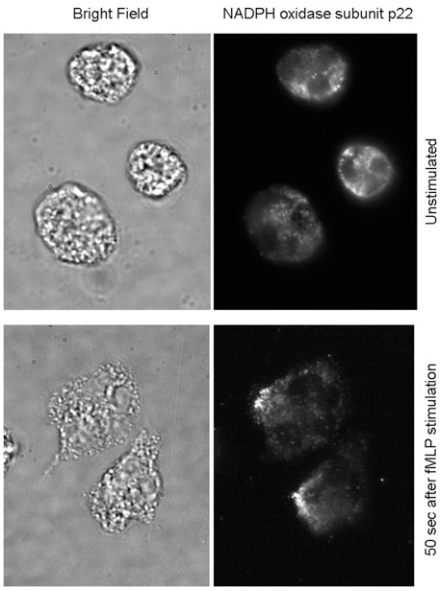

Fig. S7. NADPH oxidase is enriched near the leading edge of chemotaxing neutrophils. Purified human neutrophils were washed once with HBSS with calcium and magnesium, and were plated onto glass coverslips coated with 10 μg/mL fibronectin for 10 min at 37 °C. Neutrophils were then stimulated with 100 nM fMLP for indicated time, fixed with 6% paraformaldehyde/PBS solution for 5 min at room temperature, and washed three times with PBS solution. Neutrophils were then permeabilized with 0.2% Triton-X in PBS solution for 10 min at room temperature and then preblocked with PBS solution/1% BSA blocking buffer for 15 min at room temperature. Primary antibody (1:1,000; rabbit anti-p22 subunit of NADPH oxidase) was then added to the fixed cells in the blocking buffer for 1 h, washed three times with PBS solution, followed by incubation with secondary antibodies (1:1,000; Alexa 488–conjugated anti-rabbit IgG) for 30 min and three washes with PBS solution. The distribution of p22 was imaged in the FITC channel.

Table S1. Summary of the primary screening

Drug effect	No. of compound
No effect	303
Cell death (lysed cells)	15
Complete inhibition of polarization & migration (intact but round cells)	18
Slow and/or "long-tailed" migration	38
Directionality defect and/or Multiple pseudopods	12
Total number	386

Other Supporting Information Files

Dataset S1 (XLS)
Dataset S2 (XLS)
Dataset S3 (XLS)

Supplemental Table 2. Drugs that do not afftect neutrophil chemotaxis. The movie files for each compound will be released to a public database after the publication of this paper.

Tag No.	Cat No.	Drug Name	Target	Concentration used
1A2	0355	(+/-)-Acetylcarnitine chloride	Intermediate in lipid metabolism	2.5mM
1H2	0384	N-Acetyl-L-leucyl-L-leucyl-L-methional	Cathepsin inhibitor	1µM
1A3	0385	SG 209	K+ channel opener	2.88mM
1C3	0414	AG 490	EGFR-kinase inhibitor. Also JAK2, JAK3 inhibitor	135µM
1D3	0415	Ro 20-1724	PDE4 inhibitor	38µM
1 E3	0416	YS-035 hydrochloride	Inhibits K+ outward / pacemaker current	300µM
1H3	0432	MY-5445	PDE5 inhibitor	5µM
1A4	0433	SC-9	Protein kinase C activator	5µM
1B4	0438	Etazolate hydrochloride	PDE4 inhibitor	20µM
1C4	0442	4-Chlorophenylguanidine hydrochloride	Urokinase inhibitor	60µM
1D4	0448	Calpeptin	Calpain and cathepsin L inhibitor	520nM
1 E4	0455	(S)-(-)-Carbidopa	Aromatic L-amino acid decarboxylase inhibitor	160µM
1F4	0462	(E)-Capsaicin	Cis isomer of E-Capsaicin	3µM
1G4	0463	(Z)-Capsaicin	Cis isomer of E-Capsaicin	3µM
1A5	0468	N1,N11-Diethylnorspermine tetrahydrochloride	Spermine and spermidine acetyltransferase potentiator	100µM
1C5	0477	(+/-)-Decanoylcarnitine chloride	Intermediate in lipid metabolism	2.5mM
1D5	0478	Flurofamide	Urease inhibitor	5µM
1 E5	0483	OR-486	Catechol-O-methyl transferase inhibitor	370nM
1F5	0485	Alrestatin	Aldehyde reductase/Aldose reductase inhibitor	580µM
1G5	0493	AG 18	EGFR/PDGFR-kinase inhibitor	350µM
1H5	0497	AG 99	EGFR kinase inhibitor	100µM
1A6	0500	N(1),N(12)-Diethylspermine tetrahydrochloride	Polyamine synthase inhibitor	100µM
1B6	0503	AG 213	EGFR/PDGFR-kinase inhibitor	30µM
1D6	0507	Dantrolene sodium salt	Ca2+ release inhibitor	100µM
1 E6	0512	SKF 91488 dihydrochloride	Histamine N-methyl transferase inhibitor	10µM
1F6	0518	EBPC	Aldose reductase inhibitor	470nM
1H6	0526	(+/-)-Hexanoylcarnitine chloride	Intermediate in lipid metabolism	2.5mM
1D7	0546	L-NIO dihydrochloride	Potent eNOS inhibitor	5µM
1F7	0552	MMPX	PDE1 inhibitor	52µM
1H7	0571	PCA 4248	PAF receptor antagonist	10.5µM
1A8	0577	Methyl 2,5-dihydroxycinnamate	EGFR-kinase inhibitor	7.7µM
1B8	0578	Tyrphostin B44	EGFR-kinase inhibitor	4µM
1C8	0579	Tyrphostin B44 (+)	EGFR-kinase inhibitor	8.6µM
1D8	0583	Minoxidil	K+ channel (KATP) opener	1.4µM
1 E8	0584	L(-)-alpha-Methyldopa	Aromatic L-amino acid decarboxylase inhibitor	100µM
1F8	0593	NPPB	Chloride channel blocker	800nM
1G8	0598	SNAP	A stable analogue of endogenous S-nitroso compounds	50µM
1B9	0602	7-Nitroindazole	Non-selective NOS inhibitor.	4.7µ
1C9	0603	SNOG	NO carrier. Breaks down to release NO	200µM
1D9	0605	(+/-)-Octanoylcarnitine chloride	Intermediate in lipid metabolism	500µM
1 E9	0606	OBAA	Phospholipase A2	700nM
1F9	0607	17-ODYA	LTB-omega-Hydroxylase inhibitor	400µM
1H9	0611	(+/-)-Propionylcarnitine chloride	Intermediate in lipid metabolism	500µM
1A10	0615	trans-4-Phenylchalcone oxide	Potent and selective inhibitor of trans-styrene oxide hydrolase	640nM
1B10	0616	AG 556	EGFR-kinase inhibitor	11µM
1C10	0618	AG 555	Potent EGFR-kinase inhibitor	7µM
1D10	0619	AG 494	Potent EGFR-kinase inhibitor	7µM
1 E10	0630	Rosmarinic acid	Antiinflammatory, cytostatic, and antiviral	1.8mM
1G10	0645	2-(1-Thienyl)ethyl 3,4-dihydroxybenzylidenecyanoacetate	5-, 12-, 15-Lipoxygenase	5µM
1H10	0650	Trimethoprim	Dihydrofolate reductase inhibitor	140µM
1A11	0652	Thalidomide	TNF-alpha synthesis inhibitor	155µM
1C11	0663	L-Arginine	Endogenous substrate for NOS	100µM
1D11	0664	L-NNA	NOS inhibitor (nNOS = eNOS >>iNOS)	30µM
1 E11	0665	L-NAME hydrochloride	Non-selective NOS inhibitor (muscarinic acetylcholine receptor antagonist)	1mM
1F11	0671	AH 6809	EP1 and EP2 receptor antagonist	3.5µM
1G11	0673	L-Canavanine sulfate	iNOS inhibitor	1mM
1H11	0674	Dequalinium dichloride	K+ channel blocker (SKCa)	11µM
2B2	0681	L-690,330	Inositol monophosphatase inhibitor	3µM
2D2	0687	Danazol	Anterior pituitary suppressant	1.16µM
2 E2	0695	Retinoic acid	Keratolytic	100µM
2F2	0708	Hydroxypropyl-beta-cyclodextrin	Widely used cyclodextrin	5mM
2G2	0710	6-Nitroindazole	nNOS inhibitor.	2.4mM
2H2	0722	N-Acetyl-N-acetoxy-4-chlorobenzenesulfonamide	Nitroxyl precursor	11.5µM
2A3	0723	Tetrindole mesylate	MAO-A	4µM
2B3	0724	Pirlindole mesylate	MAO-A	5µM
2C3	0727	Pyrrolidinedithiocarbamate Ammonium	Inhibits NFkappaB, prevents increase in NOS mRNA	410µM
2D3	0735	3-Bromo-7-nitroindazole	Selective nNOS inhibitor	8.6µM
2G3	0746	Zinc protoporphyrin IX	Haem oxygenase and guanylyl cyclase inhibitor	500nM
2H3	0747	Tin protoporphyrin IX dichloride	Haem oxygenase inhibitor	100µM
2B4	0756	SIN-1 chloride	Water soluble NO donor	1mM
2D4	0759	Castanospermine	Glucosidases alpha and beta	100µM
2 E4	0760	AM 580	Retinoic acid agonist	3.4nM
2F4	0761	TTNPB	Retinoic acid agonist	100nM
2H4	0771	L-NMMA	Non-selective NOS inhibitor	70µM
2A5	0772	Carboxy PTIO potassium salt	Stable, water soluble deactivator of NO	300µM
2B5	0776	(S)-Methylisothiourea sulfate	Highly selective iNOS inhibitor	60µM
2C5	0786	MCI-186	Anti-ischaemic agent, and antioxidant	300µM
2D5	0787	Aminoguanidine hydrochloride	Irreversible iNOS inhibitor	1.5mM
2 E5	0788	3-Aminobenzamide	PARP inhibitor	400µM
2F5	0800	7-NINA	Water soluble sodium salt of (0602)	1mM
2G5	0825	Clofibric acid	PPAR agonist	12µM
2H5	0836	ICI 185,282	Potent thromboxane receptor antagonist	1µM
2A6	0837	ICI 192,605	Potent thromboxane A2 / TP receptor antagonist	1µM
2B6	0839	DHBP dibromide	Ca2+ release inhibitor(interaction with ryanodine receptor)	48.6µM
2C6	0847	Statil	Aldose reductase inhibitor	23µM
2D6	0871	AMT hydrochloride	Potent, selective iNOS inhibitor (isoform II selective)	36nM
2 E6	0873	EIT hydrobromide	Selective iNOS inhibitor, acts arginine binding site (isoform II selective)	130nM
2F6	0876	AM 92016 hydrochloride	K+ channel blocker (KV)	300nM
2G6	0880	1H-[1,2,4]Oxadiazolo[4,3-a]quinoxalin-1-one	Selective inhibitor of NO-sensitive guanylyl cyclase	200nM
2H6	0882	ZM 226600	KATP channel opener	5µM
2A7	0897	S-Isopropylisothiourea hydrobromide	iNOS inhibitor, acts arginine binding site	98nM
2B7	0905	(S)-(-)-Rolipram	Less active enantiomer of (0905), PDE4 inhibitor	20µM
2D7	0915	Cilostamide	PDE3 inhibitor(PDE3A/PDE3B)	570nM

2 E7	0919	TRIM	nNOS / iNOS inhibitor	270µM
2F7	0934	Olvanil	Potent vanilloid receptor agonist/anandamide uptake blocker	90µM
2G7	0940	4-Aminopyridine	K+ channel blocker	100µM
2H7	0942	NS 398	Selective Cox-2 inhibitor	38µM
2A8	0947	Zaprinast	PDE5/6/9/11 inhibitor	120µM
2B8	0951	2-Iminopiperidine hydrochloride	Selective iNOS inhibitor	100µM
2C8	0960	Piroxicam	Cyclooxygenase (COX-1) inhibitor	300µM
2D8	0963	9-AC	Chloride transport inhibitor	1mM
2 E8	0970	Cycloheximide	Inhibitor of protein synthesis	50µM
2G8	1000	ZD 7288	Sino-atrial node function modulator (If inhibitor)	3µM
2H8	1014	QX 314	Na+ channel blocker	24µM
2A9	1037	PD 153035 hydrochloride	EGFR kinase inhibitor	290pM
2B9	1041	1-EBIO	Activator of epithelial KCa channels	4.9mM
2C9	1042	N-Methyllidocaine iodide	Enhances biosynthesis of phosphatidylinositol	1.3mM
2D9	1043	QX 222	Na+ channel blocker	280µM
2 E9	1046	Zardaverine	PDE3/4 inhibitor	8µM
2F9	1047	ICI 182,780	Oestrogen receptor antagonist	2.9nM
2G9	1075	Nifedipine	Ca2+ channel blocker (L-type)	35nM
2H9	1076	Ouabain	Na+,K+-ATPase	30nM
2A10	1089	8-Bromo-cGMP, sodium salt	cGMP analogue	1µM
2B10	1093	Pirfenidone	Antifibrotic agent	5mM
2C10	1095	(R)-(-)-Deprenyl hydrochloride	MAO-B inhibitor	100µM
2D10	1097	Taxol	Promotes assembly and inhibits disassembly of microtubules	10nM
2F10	1099	Forskolin	Adenylyl cyclase activator	100µM
2G10	1100	Camptothecin	DNA topoisomerase (TOPI)	255µM
2H10	1101	Cyclosporin A	Calcineurin inhibitor	50nM
2A11	1103	Ketoconazole	Cytochrome P450c17 inhibitor	12.3µM
2B11	1110	Genistein	EGFR-kinase, topoisomerase kinase inhibitor	25µM
2C11	1114	CGP 37157	Antagonist of mitochondrial Na+/Ca2+ exchange	4µM
2D11	1125	Quercetin	Non-selective PI 3-kinase inhibitor	110µM
2 E11	1126	Dexamethasone	Anti-inflammatory glucocorticoid	100nM
2F11	1130	LY 294002 hydrochloride	Selective PI 3-kinase inhibitor	14µM
2G11	1135	Spermine NONOate	Slow NO releasing agent	62µM
2H11	1139	L-NIL hydrochloride	Selective iNOS inhibitor	33µM
3A2	1140	8-Bromo-cAMP, sodium salt	Cell-permeable cAMP analogue	1mM
3C2	1144	U0126	Potent, selective inhibitor of MEK1 and 2	700nM
3 E2	1148	Siguazodan	PDE3 inhibitor	1.17µM
3F2	1200	N(omega)-Propyl-L-arginine	Highly selective inhibitor of nNOS	570nM
3G2	1202	SB 203580	Selective inhibitor of p38 MAPK(SAPK2a/p38, SAPK2b/p38b2)	5µM
3H2	1206	SC 19220	Selective EP1 receptor antagonist	67µM
3B3	1222	DMPQ dihydrochloride	Potent inhibitor of beta-type PDGFRTK	800nM
3D3	1226	Etoposide	Topoisomerase II inhibitor	592µM
3G3	1229	Actinomycin D	Antineoplastic antibiotic (inhibit RNA synthesis)	76nM
3H3	1230	Methotrexate	Cytotoxic agent (inhibit DNA synthesis)	100nM
3A4	1231	Brefeldin A	Disrupts protein translocation to Golgi	2µM
3B4	1232	Wortmannin	Potent, irreversible inhibitor of PI 3-kinase	24nM
3C4	1233	Cytochalasin D	Disrupts actin filament function	20nM
3 E4	1235	Cyclopiazonic acid	Inhibitor of SERCA ATPase	8µM
3F4	1236	BHQ	Inhibitor of SERCA ATPase	10µM
3G4	1244	KB-R7943 mesylate	Na+/Ca2+ exchange inhibitor	7µM
3A5	1257	Vincristine sulfate	Disrupts microtubules	850nM
3B5	1258	1-Deoxynojirimycin	Glucosidase I and II inhibitor	70µM
3C5	1259	1-Deoxymannojirimycin hydrochloride	alpha-Mannosidase I inhibitor	60µM
3 E5	1264	SB 202190	Potent, selective inhibitor of p38 MAPK (p38alpha/p38beta)	1µM
3F5	1267	Pifithrin-a hydrobromide	P53 inhibitor	100µM
3H5	1276	AG 1478 hydrochloride	Highly potent EGFR kinase inhibitor	30nM
3A6	1283	ARL 67156	Ecto-ATPase	1mM
3B6	1284	Olomoucine	Cyclin-dependent kinase inhibitor	70µM
3C6	1290	Anisomycin	Protein synthesis inhibitor (block translation)	10µM
3D6	1300	LFM-A13	Potent, selective BTK inhibitor	25µM
3 E6	1304	BW-B 70C	5-Lipoxygenase inhibitor	300µM
3F6	1305	Monastrol	Selective inhibitor of mitotic kinesin Eg5	140µM
3G6	1307	Ciglitazone	Selective PPARgamma agonist	30µM
3H6	1310	UCL 1684	Non-peptidic blocker of the apamin-sensitive Ca2+-activated K+ channel.	7.62nM
3A7	1311	MK 886	Inhibitor of 5-lipoxygenase-activating protein	300nM
3B7	1312	WY 14643	Selective PPARalpha agonist	6.3µM
3C7	1321	ZM 336372	Potent, selective c-Raf inhibitor	700nM
3D7	1323	Butabindide oxalate	CCK-inactivating serine peptidase inhibitor	70nM
3 E7	1326	BADGE	PPAR gamma antagonist	55µM
3F7	1349	(R)-(-)-Rolipram (-)?	More active enantiomer of (0905)	24nM
3G7	1350	(S)-(-)-Rolipram (+)?	Less active enantiomer of (0905)	500nM
3H7	1355	P1075	Potent KATP channel opener	75nM
3B8	1367	ZM 39923	Potent, selective Jak3 inhibitor	794nM
3C8	1377	Cromakalim	KATP channel opener. Active enantiomer of (1377)	210nM
3D8	1378	Levcromakalim	KATP channel opener. Active enantiomer of (1377)	4.9µM
3 E8	1381	GW 5074	Potent, selective cRaf1 kinase inhibitor	90nM
3F8	1397	PP 1	Potent, selective Src inhibitor	60nM
3G8	1398	Kenpaullone	Potent cyclin-dependent kinase inhibitor(CDK1/cyclinB, GSK-3beta)	4µM
3H8	1399	CP 339818 hydrochloride	Non-peptide, potent Kv1.3 channel blocker(Kv1.3, Kv1.4)	3µM
3A9	1400	SCH 202676 hydrobromide	Allosteric inhibitor of ligand binding to G protein-coupled receptors	18µM
3B9	1401	NU 1025	Potent PARP inhibitor	4µM
3C9	1402	SB 203580 hydrochloride	Water soluble salt of (1202) (SAPK2a/p38, SAPK2b/p38beta2)	5µM
3D9	1403	FPL 64176	Potent activator of L-type Ca2+ channels	160nM
3F9	1407	PP 2	Potent, selective Src inhibitor	50nM
3G9	1412	(-)-[3R,4S]-Chromanol 293B	IKs blocker. Enantiomer of (1412) and Icftr (CFTR chloride current) blocker	190µM
3H9	1415	1400W dihydrochloride	Potent, highly selective iNOS inhibitor	70nM
3A10	1416	Homoharringtonine	Inhibitor of protein synthesis. Antileukemic	9.2µM
3B10	1417	Daidzein	Arrests cell cycle in G1 phase.	78.6µM
3C10	1418	Resveratrol	Anti-tumour and anti-oxidant agent	230µM
3 E10	1426	PPT	Subtype selective ERa agonist	2nM
3F10	1430	DuP 697	Cyclooxygenase (COX-2) inhibitor	100nM
3H10	1439	Ruthenium Red	Blocks Ca2+ release from mitrochondia and intracellular stores	1µM
3A11	1442	BMY 45778	Non-prostanoid prostacyclin IP receptor partial agonist.	350nM
3B11	1459	SU 4312	Potent inhibitor of VEGFR tyrosine kinase/PDGFR tyrosine kinase	8µM
3D11	1461	Linomide	Immunomodulator with antitumour properties.	300µM
3 E11	1467	Daunorubicin hydrochloride	Anticancer agent	50µM
3F11	1470	Flecainide acetate	Cardiac Na+ channel blocker. Antiarrhythmic(stimulated/resting)	410µM
3G11	1475	(-)-[3R,4S]-Chromanol 293B	IKs blocker. Enantiomer of (1412)	13.6µM

3H11	1479	Mifepristone	Progesterone and glucocorticoid antagonist	50μM
4A2	1494	DPN	Highly potent ERbeta agonist	8.5nM
4B2	1496	SP 600125	Novel and selective JNK inhibitor	900nM
4C2	1503	Pinacidil	K+ channel opener. Activates KATP Channels	12.6μM
4D2	1504	Milrinone	PDE3 inhibitor	560nM
4 E2	1505	Mycophenolic acid	Immunosuppresant	1μM
4F2	1507	FR 122047	Cyclooxygenase (COX-1) inhibitor	280nM
4G2	1508	GW 9662	Selective PPARgamma antagonist	33nM
4H2	1509	TMS	Cytochrome P450 1B1 inhibitor	60nM
4A3	1510	Ozagrel hydrochloride	Selective thromboxane A2 synthetase inhibitor	40nM
4B3	1526	Mevastatin	HMG-CoA reductase inhibitor	1μM
4C3	1530	Lovastatin	Potent, competitive inhibitor of HMG-CoA	6nM
4D3	1531	Icilin	Activates a novel cold receptor. Cooling agent	3.6μM
4H3	1544	(±)-Bay K 8644	Ca2+-channel activator (L-type)	173nM
4A4	1546	(S)-(-)-Bay K 8644	Ca2+-channel activator (L-type)	100nM
4B4	1547	NSC 95397	Selective Cdc25 dual specificity phosphatase inhibitor against Cdc25A,-B,-C	960nM
4 E4	1555	AG 825	EGFR-kinase inhibitor, selective for Her2	1.5μM
4F4	1580	Purvalanol A	Cyclin-dependent kinase inhibitor(cdc2/cyclinB, cdk2/cyclinA, cdk2/cyclinE, cdk4/cyclinD1, cdk5-p35)	8.5μM
4G4	1581	Purvalanol B	Cyclin-dependent kinase inhibitor(cdc2/cyclinB, cdk2/cyclinA, cdk2/cyclinE, cdk5-p35)	90nM
4H4	1603	NKH 477	Water-soluble adenylyl cyclase activator	326nM
4B5	1614	SB 431542	Potent and selective inhibitor of TGF-beta type 1 receptor activin receptor-like kinase ALK5	940nM
4C5	1615	SB 366791	Potent, selective, competitive VR1 antagonist	6.519μM
4D5	1616	SB 216763	Potent selective GSK-3 inhibitor (alpha)	90nM
4 E5	1617	SB 415286	Potent selective GSK-3 inhibitor (alpha)	310nM
4F5	1620	Alprostadil	Prostaglandin. Vasodilator and anti-platelet agent in vivo (EP3&EP4 receptors blocker)	21nM
4G5	1621	Streptozocin	DNA alkylator; antitumour and induces diabetes	100μM
4A6	1634	Y 29794 oxalate	Prolyl endopeptidase inhibitor	9.5nM
4B6	1638	U 18666A	Inhibitor of hedgehog (hh) signalling. Also inhibits cholesterol synthesis	320nM
4F6	1657	Ginkgolide B	PAF receptor antagonist	13μM
4G6	1664	GW 1929	Selective PPARg agonist. Orally active	89nM
4H6	1672	RU 28318, potassium salt	Potent, selective mineralocorticoid receptor antagonist	1mM
4B7	1676	T 0156 hydrochloride	Highly potent, selective PDE5 inhibitor	2.3nM
4C7	1677	GW 7647	Highly selective, potent PPARa agonist. Orally active	60nM
4D7	1690	SCH 28080	H+,K+-ATPase inhibitor	200nM
4 E7	1692	Cilostazol	PDE3A inhibitor. Also adenosine uptake inhibitor	2μM
4F7	1694	Ibudilast	PDE inhibitor (non-selective)(Ia, II, III, IV, V)	480μM
4G7	1697	Noscapine hydrochloride	Tubulin inhibitor; induces apoptosis (inhibit stimulated PI turnover)	100μM
4H7	1698	L-655,240	Potent, selective thromboxane A2/prostaglandin endoperoxide antagonist	70nM
4A8	1706	Acetaminophen	Cyclooxygenase (COX-3) inhibitor	4.6mM
4C8	1708	Indomethacin	Cyclooxygenase inhibitor (COX-1 > COX-2)	6.3μM
4F8	1748	MG 132	Inhibits NF-kB activation; proteasome and calpain inhibitor.	12μM
4G8	1758	PETCM	Activator of caspase-3	200μM
4H8	1759	Nilutamide	Androgen receptor antagonist. Orally active	5μM
4B9	1761	Baicalein	5- and 12-Lipoxygenase inhibitor	95μM
4C9	1762	Acifran	Hypolipidemic agent; agonist for the HM74A receptor	21μM
4D9	1769	Flurbiprofen	Cyclooxygenase inhibitor(COX-1 and COX-2)	4μM
4 E9	1770	Deguelin	Anticancer and antiviral agent	110nM
4F9	1777	Arctigenin	Inhibitor of IkBa phosphorylation	100nM
4H9	1794	Ro 26-4550 trifluoroacetate	Competitive reversible inhibitor of interleukin-2 (IL-2) binding to its receptor	30μM
4A10	1804	SR 2640 hydrochloride	Potent, selective LTD4 /LTE4 receptor antagonist	230nM
4B10	1806	SR 33805 oxalate	Ca2+ channel blocker; binds allosterically to distinct site on L-type channels	8.9nM
4D10	1808	E-4031 dihydrochloride	Selective blocker of HERG K+ channels	78μM
4 E10	1813	Indirubin-3'-oxime	GSK-3b inhibitor	1.9μM
4F10	1816	ICI 63197	PDE4 inhibitor	350nM
4G10	1819	Demethylasterriquinone B1	Selective insulin RTK activator	60μM
4H10	1821	YM 976	Orally active PDE4 inhibitor.	22nM
4A11	1850	EXO 1	Reversible inhibitor of vasicular trafficking between endoplasmic reticulum and Golgi apparatus	200μM
4C11	1856	L-165,041	Potent PPARd agonist	60nM
4D11	1862	PRIMA-1	Restores mutant p53 activity; induces apoptosis	20μM
4 E11	1866	MRS 1845	Potent SOC inhibitor; blocks intracellular Ca2+ release	17μM
4H11	1937	NSC 693868	Cdk inhibitor. Also inhibits GSK-3(cdk1/cyclinB, cdk5/p25, GSK-3)	10μM
5B2	1942	o-3M3FBS	Inactive analogue of m-3M3FBS	100μM
5C2	1949	L-670,596	Potent and selective thromboxane A2/prostaglandin endoperoxide receptor antagonist	55nM
5D2	1956	Bestatin	Aminopeptidase inhibitor	1.62μM
5 E2	1958	GR 32191 hydrochloride	Potent thromboxane A2/TP receptor antagonist	3μM
5F2	1959	GW 311616 hydrochloride	Potent and selective inhibitor of human neutrophil elastase.	220nM
5G2	1962	SB 239063	Potent, selective p38 MAP kinase inhibitor; orally active	440nM
5A3	1965	Simvastatin	HMG-CoA reductase inhibitor	10μM
5B3	1969	SL 327	Selective inhibitor of MEK1 and MEK2	2.2μM
5C3	1975	6-Iodonordihydrocapsaicin	Potent, competitive vanilloid receptor antagonist	100nM
5D3	1991	MPP dihydrochloride	Highly selective ERa antagonist	27nM
5F3	2000	XE 991 dihydrochloride	Potent and selective blocker of KCNQ voltage-gated potassium channels	9.8μM
5H3	2004	Isradipine	Potent and selective L-type voltage-gated Ca2+ channel blocker	14nM
5A4	2006	Paxilline	Potent blocker of high-conductance Ca2+-activated K+ channels	19nM
5B4	2007	Fluticasone propionate	High affinity, selective glucocorticoid receptor agonist	37nM
5C4	2008	SKF 86002 dihydrochloride	Inhibitor of p38 MAP kinase	10μM
5D4	2020	Ch 55	Highly potent synthetic retinoid that has high affinity for RAR-a and RAR-b receptors	10nM
5F4	2022	SR 202	Selective PPARg antagonist; antidiabetic and antiobesity agent	1.4mM
5G4	2025	Cinalukast	Potent, selective CysLT1 (LTD4) leukotriene receptor antagonist	64nM
5H4	2072	Aminopurvalanol A	Cell-permeable cyclin-dependent kinase inhibitor	330nM
5A5	2076	Y-26763	KATP channel opener and active metabolite of Y-27152	270nM
5B5	2077	Y-27152	Prodrug of the KATP channel opener Y-26763	1μM
5C5	2088	DMNB	Inhibitor of DNA-dependent protein kinase (DNA-PK)	150μM
5 E5	2095	PNU 37883 hydrochloride	Novel antagonist selective for the vascular form of KATP channel	6.5nM
5F5	2097	SKI II	Selective non-lipid inhibitor of sphingosine kinase	5μM
5H5	2137	2,3-DCPE hydrochloride	Selective induces apoptosis and down-regulates Bcl-XL protein expression	126μM
5A6	2140	LY 171883	Selective, orally active leukotriene D4 (LTD4) antagonist	6.3μM
5B6	2147	Nicorandil	KATP channel opener and NO donor	100μM
5C6	2150	nTZDpa	Potent, selective non-thiazolidinedione PPARg partial agonist	2.85μM
5 E6	2152	NSC 625987	CDK-4(cdk4/cyclinD1) inhibitor	2μM
5A7	2172	AZ 10417808	Selective non-peptide inhibitor of caspase-3	149μM
5C7	2183	ZK 164015	Potent estrogen receptor silent antagonist	250nM
5D7	2184	SN-6	Selective Na+/Ca2+-exchange (NCX) inhibitor	160μM
5F7	2186	CMPD-1	Non-ATP-competitive, selective inhibitor of p38a-mediated MK2a phosphorylation	3.3μM
5G7	2192	4-HQN	Inhibitor of poly(ADP-ribose) polymerase (PARP)	95μM
5A8	2202	Zatebradine hydrochloride	Bradycardic agent that produces use-dependent inhibition of hyperpolarisation-activated current (If)	4.8μM
5B8	2208	LY 255283	Selective, competitive antagonist of BLT2 receptors	10μM
5C8	2227	CI 976	Selective acyl-coenzyme A:cholesterol acyltransferase (ACAT) inhibitor	730nM

5 E8	2229	GW 0742	Potent and highly selective PPARd agonist	10nM
5F8	2239	GW 583340 dihydrochloride	Potent dual EGFR/ErbB-2 tyrosine kinase inhibitor	1.1µM
5G8	2251	Cisplatin	Potent anticancer agent that blocks DNA synthesis	100µM
5H8	2252	Doxorubicin hydrochloride	Antitumour antibiotic agent that inhibits DNA topoisomerase II	26.1µM
5A9	2266	DY131	Novel selective agonist at estrogen-related receptors ERRb and ERRg	30µM
5B9	2271	GW 6471	PPARa antagonist that inhibits activation	2.4µM
5C9	2275	TBB	A cell-permeable selective inhibitor of casein kinase-2 (CK2)	16µM
5D9	2280	Raloxifene hydrochloride	Selective estrogen receptor modulator (SERM) that binds to ERa and Erb	10nM
5 E9	2294	Cordycepin	Nucleoside analogue that acts as an anticancer and antifungal agent	320µM
5F9	2301	T 0070907	Potent and selective PPARg antagonist	10nM
5G9	2313	QX 314 chloride	Membrane impermeable blocker of voltage-activated Na+ channels	500µM
5H9	2318	Pravastatin sodium salt	Water-soluble, competitive inhibitor of 3-hydroxy-3-methyl coenzyme A reductase	10nM
5A10	2324	Necrostatin-1	Blocks non-apoptotic cell death via inhibition of a specific cellular pathway	4.94µM
5B10	2330	DMP 543	K+ channel blocker and acetylcholine release stimulator	7µM

Supplemental Table 3. Drugs that lead to cell death (lysed cells).

Tag No.	Drug Name	Drug Target	IC50	phenotype (10xIC50)	phenotype (5xIC50)	phenotype (2xIC50)	phenotype (1xIC50)	phenotype (0.5xIC50)	phenotype (0.2xIC50)
1 E7	(+/-)-Lauroylcarnitine chloride	Intermediate in lipid metabolism	250µM	cell death	cell death	partially inhibited	partially inhibited	partially inhibited	partially inhibited
1G7	(+/-)-Myristoylcarnitine chloride	Intermediate in lipid metabolism	250µM	cell death	cell death	cell death	cell death	slow migration	no effect
1G9	(+/-)-Palmitoylcarnitine chloride	Protein kinase C inhibitor	30µM	cell death	cell death	cell death	no effect	no effect	no effect
1B11	Verapamil hydrochloride	Ca2+ channel blocker (L-type)	62µM	cell death	cell death	no effect	no effect	no effect	no effect
2C2	Diltiazem hydrochloride	Ca2+ channel blocker (L-type)	320µM	cell death	cell death	cell death	no effect	no effect	no effect
2C7	Glibenclamide	K+ channel blocker (KATP)/CFTR Cl- channel blocker	20µM	cell death	completely inhibited	partially inhibited	no effect	no effect	no effect
2F8	Tamoxifen citrate	Oestrogen receptor partial agonist / antagonist	8µM	cell death	cell death	slow & long-tailed	no effect	no effect	no effect
2 E10	Tranilast	Anti-allergic, inhibits release from mast cells(anti-AT1 receptor?)	100µM	cell death	no effect	no effect	no effect	no effect	no effect
3D4	A23187	Calcium ionophore	1.9µM	cell death	cell death	cell death	cell death	cell death	cell death
3C11	PACOCF3	Phospholipase A2 inhibitor	3.8µM	cell death	cell death	no effect	no effect	no effect	no effect
4G3	Splitomicin	Histone deacetylase (Sir2p) inhibitor	60µM	cell death	no effect	no effect	no effect	no effect	no effect
4C6	AY 9944 dihydrochloride	Inhibitor of hedgehog (hh) signaling. Inhibits D7-dehydrocholesterol reductase	210µM	cell death	cell death	cell death	completely inhibited	no effect	no effect
5A2	m-3M3FBS	Phospholipase C activator	10µM	cell death	no effect	no effect	no effect	no effect	no effect
5F6	Embelin	Cell-permeable inhibitor of X-linked inhibitor of apoptosis (XIAP)	4.1µM	cell death	cell death	no effect	no effect	no effect	no effect
5D8	Leflunomide	Immunosuppressant agent.	100µM	cell death	cell death	cell death	no effect	no effect	no effect

Supplemental Table 4. Drugs that affect neutrophil chemotaxis . The movie files for each compound will be released to a public database after the publication of this paper.

Drugs that lead to slow and/or "long-tailed" migration (38 drugs)

Tag No.	Drug Name	Drug Target	IC50	Phenotype (10xIC50)	Phenotype (5xIC50)	Phenotype (2xIC50)	Phenotype (1xIC50)	Phenotype (0.5xIC50)
1B2	W-13 hydrochloride	Calmodulin antagonist	68μM	cell death	cell death	completely inhibited	very slow migration	very slow migration
1C2	A-3 hydrochloride	Protein kinase inhibitor	135μM	cell death	cell death	cell death	completely inhibited	very slow migration
1 E2	W-7 hydrochloride	Calmodulin antagonist	51μM	cell death	cell death	completely inhibited	completely inhibited	very slow migration
1G2	A-7 hydrochloride	Calmodulin antagonist	3μM	completely inhibited	completely inhibited	slow migration	slow migration	no effect
1B3	H-9 dihydrochloride	Protein kinase inhibitor	70μM	slow migration	slow & long-tailed	slow & long-tailed	slow migration	partially inhibited
1G3	ML 9 hydrochloride	Myosin light chain kinase inhibitor	4μM	completely inhibited	slow migration	slow migration	no effect	no effect
1G6	Flunarizine dihydrochloride	Dual Na+ / Ca2+ channel (T-type) blocker	4μM	slow & long-tailed	no effect	no effect	no effect	no effect
1A7	Fasudil hydrochloride	Inhibitor of cyclic nucleotide dependent protein kinases	10.7μM	slow & long-tailed	slow & long-tailed	slow & long-tailed	slightly long-tailed	no effect
1B7	H-7 dihydrochloride	Protein kinase inhibitor (PKC, PKG, PKA, MLCK)	6μM	long-tailed migration	long-tailed migration	no effect	no effect	no effect
1C7	C-1	Protein kinase C inhibitor	64μM	completely inhibited	slow migration	slow & long-tailed	slow & long-tailed	slow & long-tailed
1F10	D-erythro-Sphingosine	Protein kinase C inhibitor	1.1μM	slow migration	no effect	no effect	no effect	no effect
2F3	Ceramide	Ser / Thr protein phosphatase activator	6μM	completely inhibited	slow migration	slow migration	no effect	no effect
2A4	Dihydrosphingosine	Protein kinase C inhibitor	2μM	slow migration	slow migration	no effect	no effect	no effect
2C4	Vinpocetine	Phosphodiesterase(PDE1) inhibitor/Na+ channel blocker	21μM	slow migration	slow migration	no effect	no effect	no effect
3A3	PD 98059	Specific inhibitor of MEK	7μM	slightly long tailed	slightly long-tailed	no effect	no effect	no effect
3C3	2APB	Membrane permeable IP3 receptor antagonist	42μM	very slow migration	slow & long-tailed	long-tailed	no effect	no effect
3 E3	Apigenin	Anticancer agent	20μM	slow & long-tailed	slow & long-tailed	slow & long-tailed	long-tailed	slightly long-tailed
3 E9	(-)-Terreic acid	Selective inhibitor of BTK(Bruton's tyrosine kinase)	30μM	slow migration	no effect	no effect	no effect	no effect
3D10	DCEBIO	Activates Cl- conductance and hIK1 K+ channels	60μM	partially inhibited	long-tailed	long-tailed	long-tailed	no effect
4C4	Cantharidin	Protein phosphatase 1 and 2A inhibitor	1.1μM	slow migration	slow migration	no effect	no effect	no effect
4D4	STO-609 acetate	Selective CaM kinase kinase inhibitor (CaM-KK alpha&beta)	214μM	slow & long-tailed	long-tailed	long-tailed	slightly long-tailed	slightly long-tailed
4A7	YM 90709	Interleukin-5 receptor antagonist	1μM	slow & long-tailed	long-tailed	no effect	no effect	no effect
4B8	Sulindac	Cyclooxygenase inhibitor (following metabolism to sulindac sulfide)	100μM	completely inhibited	completely inhibited	very slow migration	slow & long-tailed	slow migration
4A9	(±)-Blebbistatin	Selective inhibitor of nonmuscle myosin II	2μM	slow & long-tailed	slow & long-tailed	no effect	no effect	no effect
4G9	Ro 106-9920	Inhibitor of NF-kB activation	3μM	completely inhibited	very slow migration	slow migration	slightly slow	no effect
4B11	(S)-(-)-Blebbistatin	Selective inhibitor of nonmuscle myosin II ATPase activity	2μM	slow & long-tailed	slow & long-tailed	slow & long-tailed	long-tailed	no effect
4F11	NSC 663284	Potent, selective inhibitor of Cdc25 dual specificity phosphatases	10μM	very slow migration	very slow migration	very slow migration	very slow migration	slow & long-tailed
4G11	BTS	Selective inhibitor of skeletal muscle myosin II ATPase activity	5μM	slow migration	slightly slow	no effect	no effect	no effect
5 E3	Linopirdine dihydrochloride	Blocker of KCNQ voltage-gated potassium channels.(KCNQ1, KCNQ2+3)	8.9μM	slow migration	no effect	no effect	no effect	no effect
5G3	Ro 31-8220 mesylate	Protein kinase C inhibitor, with activity at other protein kinases	38nM	slow & long-tailed	slow migration	slower migration	no effect	no effect
5D6	API-2	Selective inhibitor of Akt (protein kinase B) signaling	46μM	slow migration	slow migration	no effect	no effect	no effect
5G6	Bax channel blocker	Potent inhibitor of Bax-mediated mitochondrial cytochrome c release	520nM	slow & long-tailed	slow & long-tailed	no effect	no effect	no effect
5B7	BVT 948	Non-competitive, cell permeable inhibitor of protein tyrosine phosphatases	7.1μM	slow at first	slow at first	slow at first	no effect	no effect
5 E7	NSC 146109 hydrochloride	Cell-permeable antitumour agent that activates p53-dependent transcription	15.8μM	cell death	cell death	cell death	slow migration	slow migration
5H7	R 59-022	Diacylglycerol kinase inhibitor	2.8μM	slow migration	slow migration	no effect	no effect	no effect
3G10	D609	Selective PC-PLC inhibitor	75μM	partially inhibited	partially inhibited	partially inhibited	partially inhibited	no effect
4 E3	DCPIB	Potent, selective blocker of the volume-sensitive anion channel (VSAC)	4.1μM	partially inhibited	partially inhibited	partially inhibited	partially inhibited	partially inhibited
5H6	INCA-6	Inhibitor of interaction between calcineurin and its substrate NFAT	800nM	partially inhibited	partially inhibited	partially inhibited	no effect	no effect

Drugs that completely inhibit polarization and migration (18 drugs)

Tag No.	Drug Name	Drug Target	IC50	Phenotype (10xIC50)	Phenotype (5xIC50)	Phenotype (2xIC50)	Phenotype (1xIC50)	Phenotype (0.5xIC50)
1D2	W-5 hydrochloride	Calmodulin antagonist	240μM	cell death	cell death	cell death	completely inhibited	completely inhibited
1F2	W-9 hydrochloride	Calmodulin antagonist	72μM	cell death	cell death	cell death	completely inhibited	completely inhibited
1F3	SC-10	Protein kinase C activator	100μM	cell death	completely inhibited	completely inhibited	completely inhibited	no effect
1H4	Capsazepine	Vanilloid receptor antagonist.	3.2μM	completely inhibited	partially inhibited	no effect	no effect	no effect
1H8	Nimodipine	Ca2+ channel blocker (L-type)	60μM	cell death	completely inhibited	completely inhibited	partially inhibited	partially inhibited
1A9	Nitrendipine	Ca2+ channel blocker (L-type)	30μM	completely inhibited	completely inhibited	partially inhibited	no effect	no effect
2A2	NPC 15199	Novel anti-inflammatory agent	36μM	completely inhibited	completely inhibited	completely inhibited	no effect	no effect
2G4	Bifemelane hydrochloride	MAO-A and MAO-B inhibitor	30μM	completely inhibited	completely inhibited	completely inhibited	slow migration	slow migration
3G5	U 73122	Phospholipase C inhibitor	5μM	completely inhibited	completely inhibited	partially inhibited	partially inhibited	partially inhibited
4F3	HA14-1	Bcl-2 inhibitor. Induces apoptosis	9μM	cell death	completely inhibited	completely inhibited	partially inhibited	partially inhibited
4A5	Rottlerin	Reported PKCd inhibitor	6μM	completely inhibited	partially inhibited	partially inhibited	no effect	no effect
4H5	NPC 15437 dihydrochloride	Selective protein kinase C inhibitor	19μM	cell death	cell death	completely inhibited	partially inhibited	slow migration
4 E6	Lonidamine	Anticancer and antispermatogenic agent. Inhibits mitochondrial hexokinase	365μM	completely inhibited	completely inhibited	completely inhibited	partially inhibited	no effect
4D8	Bay 11-7085	Irreversible inhibitor of TNF-a-induced IkBa phosphorylation	10μM	completely inhibited	completely inhibited	completely inhibited	completely inhibited	slow migration
4 E8	Bay 11-7821	Irreversible inhibitor of TNF-a-induced IkBa phosphorylation	10μM	completely inhibited	completely inhibited	completely inhibited	completely inhibited	slow migration
5H2	Gossypol	Anticancer, antifertility agent	7μM	completely inhibited	partially inhibited	no effect	no effect	no effect
5D5	RS 102895 hydrochloride	CCR2b-selective chemokine receptor antagonist	17.8μM	completely inhibited	slow migration	no effect	no effect	no effect
5G5	Apoptosis Activator 2	Apoptosis activator	9μM	completely inhibited	partially inhibited	no effect	no effect	no effect

Drugs that lead to directionality defect and/or multiple pseudopods (12 drugs)

Tag No.	Drug Name	Drug Target	IC50	Phenotype (10xIC50)	Phenotype (5xIC50)	Phenotype (2xIC50)	Phenotype (1xIC50)	Phenotype (0.5xIC50)
1B5	2,4-Diamino-6-hydroxypyrimidine	Inhibits biosynthesis of tetrahydrobiopterin and thus NOS	300μM	cell death	completely inhibited	partially inhibited	random movement	random movement
1C6	Diphenyleneiodonium chloride	Binds to flavoproteins and inhibits NADPH oxidase	10μM	multiple pseudopods	multiple pseudopods	multiple pseudopods	multiple pseudopods	no effect
2 E3	GF 109203X	Protein kinase C inhibitor(α/β1/γ/δ/ε/ζ subtypes)	5.8μM	completely inhibited	head shaking	random movement	multiple pseudopods	no effect
3B2	Dibutyryl-cAMP, sodium salt	Cell-permeable cAMP analogue	100μM	head shaking	slightly head shaking	no effect	no effect	no effect
3D2	SKF 96365 hydrochloride	Receptor-operated calcium channel blocker	11.2μM	random movement	random movement	random movement	no effect	no effect
3F3	Nocodazole	Microtubule inhibitor	3.2μM	long-tailed	multiple pseudopod	multiple pseudopod	random movement	random movement
3H4	Vinblastine sulfate	Disrupts microtubules	178nM	slightly random	slight random	slightly random	slightly random	no effect
3D5	EHNA hydrochloride	Adenosine deaminase inhibitor	4μM	multiple pseudopods	multiple pseudopods	slow migration	no effect	no effect
3A8	Colchicine	Inhibitor of tubulin	1μM	random movement	slightly random	slightly random	slightly random	slightly random
4D6	D-64131	Inhibitor of tubulin polymerization. Antitumour in vivo	74nM	random movement	slightly random	no effect	no effect	no effect
4C10	2-Methoxyestradiol	Apoptotic and antiangiogenic agent (inhibits tubulinpolymerization)	1.9μM	random movement	no effect	no effect	no effect	no effect
5 E4	LE 135	Retinoic acid antagonist	1.4μM	multiple pseudopods	multiple pseudopods	multiple pseudopods	multiple pseudopods	multiple pseudopods